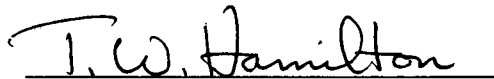


Technical Report No. 32-412

Moon-to-Earth Trajectories

S. S. Dallas

A handwritten signature in cursive script, reading "T. W. Hamilton", is positioned above a horizontal line.

T. W. Hamilton, Chief
Systems Analysis Section

**JET PROPULSION LABORATORY
CALIFORNIA INSTITUTE OF TECHNOLOGY
PASADENA, CALIFORNIA**

June 1, 1963

Copyright © 1963
Jet Propulsion Laboratory
California Institute of Technology

Prepared Under Contract No. NAS 7-100
National Aeronautics & Space Administration

CONTENTS

I. Introduction	1
II. Lunar Return Trajectory Characteristics	2
A. Keplerian Presentation of the Lunar Return Geometry	2
B. Types of Lunar Return Ascent Trajectories	11
C. Rendezvous Return	15
III. Trajectory-Computing Techniques	16
A. Analytic Lunar Return Program	16
B. Space Trajectories Program	16
C. Search Parameters	16
D. Search Technique	17
IV. A Typical Set of Lunar Return Trajectories	19
A. Design Constraints	19
B. Trajectory Characteristics	19
1. Ascent Trajectory	19
2. Transfer Orbit	22
3. Re-entry Trajectory	22
C. Launch-on-Time Theory	23
Nomenclature	44
References	46

TABLES

1. Selenocentric injection conditions and major-body angles	6
2. Characteristics of the selenocentric hyperbola	7
3. Characteristics of the point of exit from the lunar sphere of influence	8
4. Characteristics of the geocentric ellipse	9
5. Characteristics of the points of re-entry and impact	10

FIGURES

1. Keplerian presentation of the lunar return geometry	3
2. Locus of asymptote piercing or exit points	4
3. In-plane angle between exit point and re-entry point vs. time of flight and energy C_{3E}	12
4. Types of lunar return trajectories	13
5. Launch site location referenced to the outward radial direction	13
6. Angle between outward radial direction and periselene vs. time of flight and energy C_{3M}	14
7. Locus of launch sites for injection at closest approach distance	15
8. Locus of launch sites for injection at positive Γ_b	15
9. Definition of the impact parameter B	17
10. Present search routine for Space Trajectories Program	18
11. Lunar tracks of the ascent trajectories, impact site, San Antonio, Texas	20
12. Lunar tracks of the ascent trajectories, impact site, Bourke, Australia	21
13. Lunar return Earth track for launch date of March 8, 1969, and landing site at San Antonio, Texas	24
14. Lunar return Earth track for launch date of March 9, 1969, and landing site at San Antonio, Texas	25
15. Lunar return Earth track for launch date of March 10, 1969, and landing site at San Antonio, Texas	26
16. Lunar return Earth track for launch date of March 11, 1969, and landing site at San Antonio, Texas	27
17. Lunar return Earth track for launch date of March 12, 1969, and landing site at San Antonio, Texas	28
18. Lunar return Earth track for launch date of March 13, 1969, and landing site at San Antonio, Texas	29
19. Lunar return Earth track for launch date of March 14, 1969, and landing site at San Antonio, Texas	30
20. Lunar return Earth track for launch date of March 15, 1969, and landing site at San Antonio, Texas	31
21. Lunar return Earth track for launch date of March 16, 1969, and landing site at San Antonio, Texas	32
22. Lunar return Earth track for launch date of March 20, 1969, and landing site at Bourke, Australia	33
23. Lunar return Earth track for launch date of March 21, 1969, and landing site at Bourke, Australia	34

FIGURES (Cont'd)

24. Lunar return Earth track for launch date of March 22, 1969, and landing site at Bourke, Australia	35
25. Lunar return Earth track for launch date of March 23, 1969, and landing site at Bourke, Australia	36
26. Lunar return Earth track for launch date of March 24, 1969, and landing site at Bourke, Australia	37
27. Lunar return Earth track for launch date of March 25, 1969, and landing site at Bourke, Australia	38
28. Lunar return Earth track for launch date of March 27, 1969, and landing site at Bourke, Australia	39
29. Lunar return Earth track for launch date of March 28, 1969, and landing site at Bourke, Australia	40
30. Lunar return Earth track for launch date of March 29, 1969, and landing site at Bourke, Australia	41
31. Lunar return Earth track for launch date of March 30, 1969, and landing site at Bourke, Australia	42
32. Launch-on-time problem	43

ABSTRACT

The design and characteristics of trajectories that initiate on the surface of the Moon and terminate at a specific landing site on the surface of the Earth are presented in this Report, along with computing techniques for such trajectories. Results from an analytic trajectory-computing program are used for the qualitative discussions, and results from a precision integrating program are used for the quantitative discussions.

I. INTRODUCTION

Moon-to-Earth trajectories, also known as lunar return trajectories, have gained in importance as a result of the recent desire to send man to the Moon and back again. As a result of intensive trajectory analysis in projects such as *Ranger* and *Surveyor*, the problem of launching from the Earth to the Moon is solved. However, the reverse problem, that of launching from the Moon and returning to the Earth, still remains to be thoroughly understood. The analysis presented in this Report is concerned with the design of trajectories that initiate upon the surface of the Moon and terminate upon the surface of the Earth. Part II describes the general characteristics of the lunar return trajectory. From these characteristics,

a set of search parameters is chosen which, when satisfied, defines an acceptable lunar return trajectory. Part III presents the IBM 7090 trajectory-computing programs and techniques used in designing a set of lunar return trajectories. Part IV defines a set of design constraints for a typical set of trajectories, presents the characteristics of this set of trajectories, and discusses the launch-on-time problem.

Definitions of terminology, symbols, and subscripts are presented in the Nomenclature. Reference to the Nomenclature is indicated by an asterisk (*).

II. LUNAR RETURN TRAJECTORY CHARACTERISTICS

A. Keplerian Presentation of the Lunar Return Geometry

In the design of *Ranger* Earth-to-Moon trajectories, a technique for understanding general geometrical relationships is used very successfully. This technique assumes that the gravitational field of the Earth-Moon system consists of two independent inverse-square force fields, one associated with the Earth and one associated with the Moon. Under this system, a trajectory consists of two Keplerian orbits,* usually elliptic in the sphere of influence* of the Earth and hyperbolic in the sphere of influence of the Moon. Since the geometrical problem of a Moon-to-Earth trajectory is similar to that of an Earth-to-Moon trajectory, the same technique is used in this Report.

Figure 1 presents a three-dimensional drawing of the Keplerian presentation of the lunar return trajectory geometry. For any given set of re-entry conditions at the Earth, two solutions exist. The first solution is a counterclockwise trajectory, one that enters the atmosphere of the Earth in the same direction as the Earth's rotation, shown as a solid line. The second solution is a clockwise trajectory, one that enters the atmosphere of the Earth in the opposite direction as the Earth's rotation, shown as a dashed line. The lunar return trajectory is approximated by two joined conic sections. The first conic section is drawn in a Moon-centered inertial system and is a hyperbolic orbit up to the piercing point* of the lunar sphere of influence (LSOI). At this point, the reference frame is changed to the Earth-centered inertial system by adding the velocity of the Moon relative to the Earth, \mathbf{V}_M , to the velocity of the probe relative to the Moon, \mathbf{V}_{PM} , and obtaining the velocity of the probe relative to the Earth, \mathbf{V}_P . The second conic section is drawn in the Earth-centered inertial system and is an elliptical orbit which terminates at the point of entry into the atmosphere of the Earth. The apparent discontinuity of the trajectory at the exit point* of the LSOI is a result of drawing the first phase of the trajectory as seen in a Moon-centered inertial system and the second phase of the trajectory as seen in an Earth-centered inertial system. If a single frame of reference is used, the actual shape of the trajectory with respect to the frame of reference chosen is presented and the discontinuity is removed, but now the trajectory is not presented as two joined conics and the general trajectory relationships can not be easily discussed. The objective of Fig. 1 is to pre-

sent the general trajectory relationships and not the actual shape of the trajectory.

It has been empirically determined that the velocity vector \mathbf{V}_{PM} is very nearly equal to the hyperbolic excess velocity vector \mathbf{V}_P at the piercing point of the LSOI. As a result, the direction of \mathbf{V}_{PM} closely represents the outward radial direction or outgoing asymptote of the selenocentric hyperbola. Since \mathbf{V}_M points to the lunar west and is approximately in the Earth-Moon plane perpendicular to the Earth-Moon line, every outward radial direction that describes a lunar return trajectory must point toward the lunar east so that the velocity with respect to the Earth at the piercing point of the LSOI points toward the Earth as shown in Fig. 1.

The exit points of the outward radial directions for a constant Earth-to-Moon distance, time of flight, and re-entry path angle form a circular locus at the LSOI with the exit point of the vertical impact outward radial direction as the center. The position and size of the locus of exit points relative to the Earth-Moon line depend upon three parameters, the Earth-to-Moon distance, the flight time, and the re-entry angle. First, as the Earth-to-Moon distance increases, the angular distance of the locus of exit points from the Earth-Moon line decreases. Second, as the flight time increases, the angular distance of the locus from the Earth-Moon line and the angular diameter of the circular locus increase. Finally, as the re-entry angle increases, the angular diameter of the locus decreases.

Figure 2 presents the locus of asymptote piercing points or exit points for lunar return trajectories having a flight time of 70 hr and a re-entry flight path angle of a negative 6 deg for a mean Earth-to-Moon distance. The outward radial direction for the lunar return trajectory which impacts upon the Earth vertically is at an angle of about 52.5 deg with the Earth-Moon line and is in the Earth-Moon plane. The outward radial direction for a clockwise re-entry trajectory is to the right of this at an angle of 57.0 deg with the Earth-Moon line and requires a maximum \mathbf{V}_{PM} (Ref. 1). The outward radial direction for a counterclockwise re-entry trajectory is to the left of the vertical impact outward radial direction at an angle of 48.0 deg with the Earth-Moon line and requires a minimum \mathbf{V}_{PM} . These two cases represent the worst and the best trajectories, respectively, from the viewpoint of required lunar boost impulse. The remaining outward

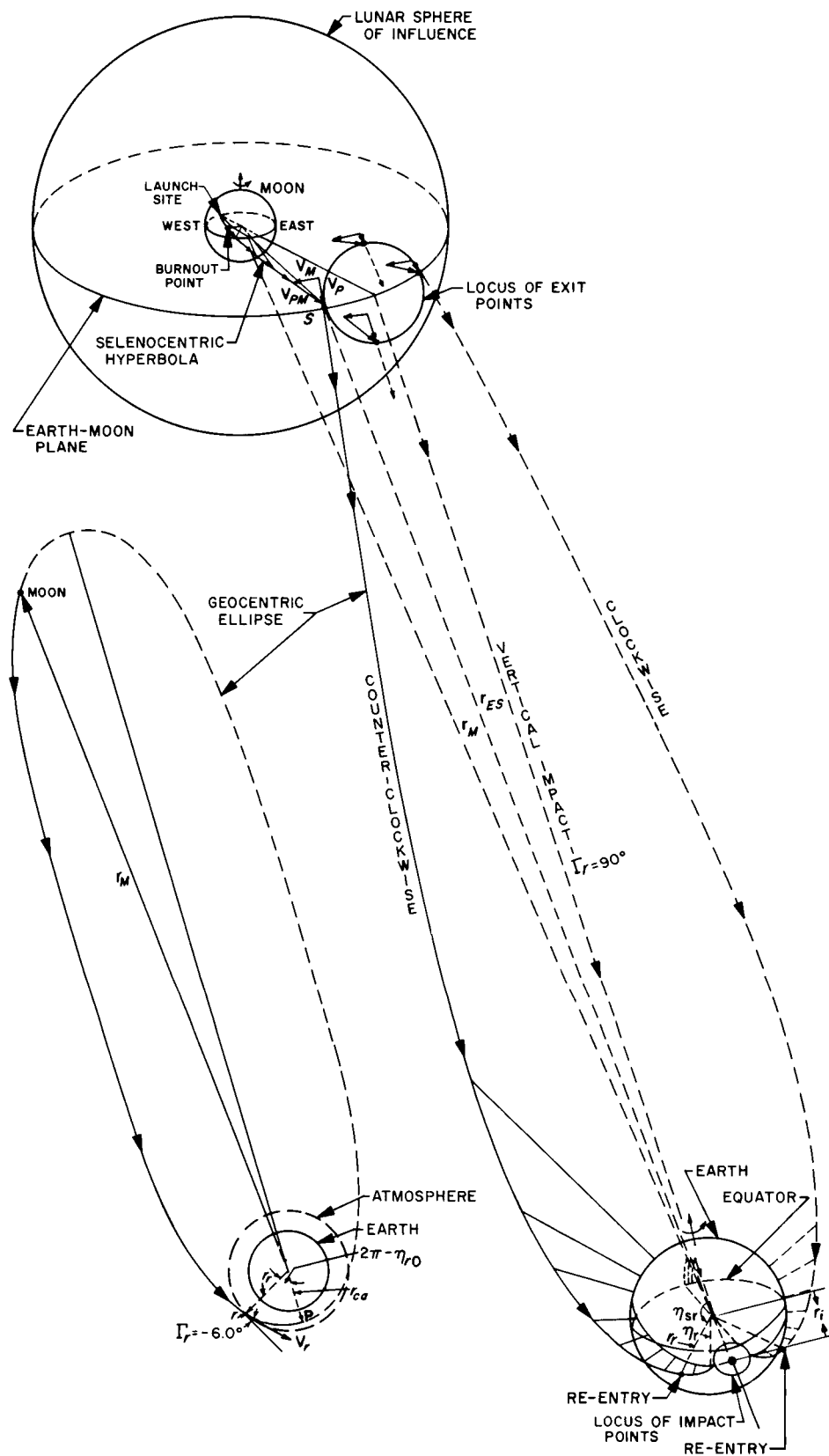


Fig. 1. Keplerian presentation of the lunar return geometry

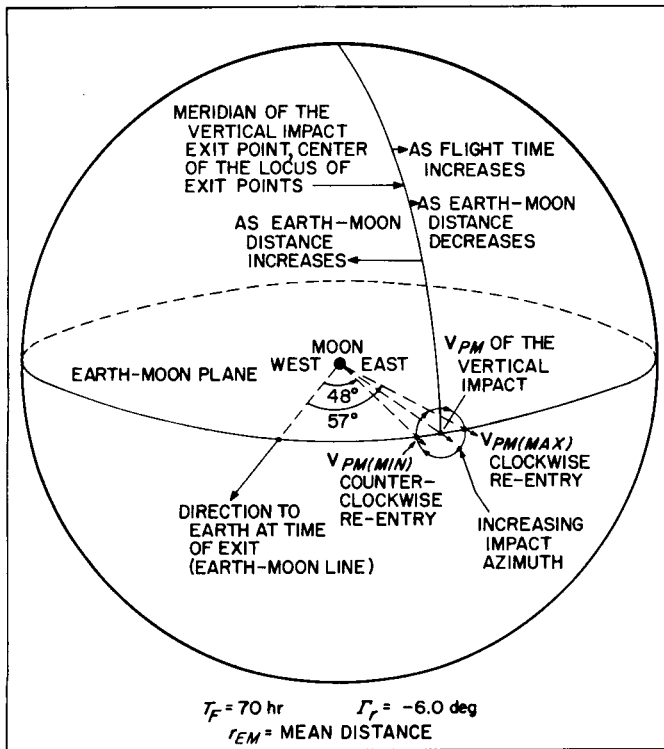


Fig. 2. Locus of asymptote piercing or exit points

radial directions exhibit impulses between these two. Consequently, the magnitude of V_{PM} is a function of the Earth-to-Moon distance, the flight time, the re-entry angle, and the direction of the trajectory (clockwise or counterclockwise).

The locus of exit points may be thought of as the locus formed by the point s as the outward radial direction is rotated about the vertical impact outward radial direction by controlling V_{PM} . Figure 1 shows that the vector from the center of the Earth to the point s , r_{Es} , rotates about the vertical impact trajectory as the locus of exit points is formed. The vertical impact trajectory is very nearly the direction of the Moon at launch since the angular momentum of the probe is cancelled by the angular momentum of the Moon during transit through the LSOI. The rotation of r_{Es} about the vertical impact trajectory forms a cone with its apex at the center of the Earth. The trajectory plane contains r_{Es} and the center of the Earth and, therefore, rotates about the vertical impact trajectory as the locus of exit points is formed. Reference 1 shows that the in-plane angle between the exit point s and the point of re-entry r , η_{sr} , is a function of the Earth-to-Moon distance (launch date), the time of flight (energy C_{3E}), and the re-entry flight path angle. Since these three parameters are defined as constant, η_{sr}

is constant. By defining a constant re-entry maneuver angle η_r , the total in-plane angle η_{si} is constant. Therefore, the impact radius vector r_i in the trajectory plane is at a constant angle of η_{si} from the vector r_{Es} . As the trajectory plane rotates about the vertical impact trajectory, the vector r_i forms a second cone with its apex at the center of the Earth and the direction of the vertical impact trajectory as its axis. The intersection of this cone with the surface of the Earth forms a circular locus of impact points. Since the outward radial direction, the vector r_{Es} , and the vector r_i are all slaved together, the locus of exit points and the locus of impact points are formed simultaneously as the trajectory plane rotates about the vertical impact trajectory according to the variation of the velocity vector V_{PM} . Hence, for each exit point on the locus of exit points there is a corresponding impact point on the locus of impact points. Figures 1 and 2 show that as the locus of exit points is traversed from maximum V_{PM} to minimum V_{PM} in a clockwise fashion, the azimuth of impact varies in an increasing fashion. Therefore, given an Earth-to-Moon distance, a time of flight, a re-entry angle, and a maneuver angle, the circular locus of impact points is defined. In addition, if a specific impact latitude is defined, then the circular locus reduces to two impact points. The first impact point is associated with a counterclockwise re-entry having an impact azimuth between 0 and 180 deg, and the second impact point is associated with a clockwise re-entry having an impact azimuth between 180 and 360 deg. The two points would differ in longitude by a $\Delta\theta$, the angular diameter of the impact cone. If a specific impact longitude is defined, there are still two possible trajectories, one counterclockwise and one clockwise. The correct impact longitude for each of the cases is obtained by varying the launch time, which is directly related to impact longitude. Varying the launch time an hour or so in order to correct impact longitude does not significantly affect the remaining trajectory characteristics.

If the re-entry angle is varied from shallow to steep angles, the angular diameter of the impact cone will increase to a maximum of 180 deg and then decrease on the Moon side of the Earth to a point corresponding to the vertical impact point, which is at a latitude equal to the declination of the Moon at the time of exit from the LSOI.

Figure 1 presents a typical manned lunar return trajectory from the lunar injection point to the impact point upon the Earth, shown as a solid line. The flight time is 70 hr, the re-entry is counterclockwise, and the re-entry path angle is a -6.0 deg. The ascent trajectory* is not

typical of a manned lunar return trajectory; however, the important near-Earth characteristics are independent of the ascent trajectory and are, therefore, typical. The trajectory after exit from the LSOI consists of a highly elliptical orbit since the flight time is 70 hr. For a flight time of 45 hr, this phase of the trajectory would be a hyperbolic conic. The clockwise re-entry trajectory is also shown. The choice of which of the two solutions is better depends upon two criteria, the amount of return-boost impulse required and the amount of re-entry retro-rocket impulse required. The previous discussions of Fig. 1 and 2 indicated that the amount of return-boost impulse required is less for the counterclockwise re-entry trajectory. In addition, the amount of retrorocket impulse required at re-entry is less for the counterclockwise re-entry trajectory since the inertial velocity of the probe relative to the rotating atmosphere in inertial space is less. For these reasons, the counterclockwise trajectory is better and is the one primarily used and discussed in this Report.

Reference 1 points out several interesting characteristics of the geocentric phase of the lunar return trajectory which are apparent in Tables 1 through 5.¹ These characteristics are summarized below.

1. For a fixed flight time, vehicles launched on those days when the Moon is farthest from the Earth must have higher energies than those launched when the Moon is closest to the Earth.

2. The effects of the re-entry path angle Γ_r , the impact site, and the direction of the trajectory (clockwise or counterclockwise) on the inertial re-entry velocity are negligible. The re-entry velocity is primarily dependent upon the flight time and the Earth-to-Moon distance.

3. The energy of the geocentric conic is a function of the Earth-to-Moon distance, the flight time, and the re-entry path angle. Trajectories having steep re-entry path angles have lower energies than trajectories with the same flight time but with shallower re-entry path angles. The trajectories with steep re-entry angles re-enter on the side of the Earth facing the Moon and require less travel distance than the trajectories with shallow re-entry angles which re-enter on the far side of the Earth.

4. The in-plane angle η_{sr} , between the exit point of the LSOI and the re-entry point at the Earth, is dependent upon the Earth-to-Moon distance, the flight time, and the re-entry angle. The re-entry radius distance is fixed at a radius distance of 6,500 km. The angle η_{sr} can also be

represented as a function of the Earth-to-Moon distance r_{EM} , the energy C_{3E} , and the re-entry flight path angle Γ_r . The energy C_{3E} is a function of the Earth-to-Moon distance, the flight time, and the re-entry angle.

From Fig. 1 and Ref. 1

$$C_{3E} \triangleq V_P^2 - \frac{2\mu_E}{r_{Es}}$$

and

$$a = \frac{\mu_E}{C_{3E}}$$

where

$$\mu_E \triangleq GM_E$$

$$r_r = 6,500 \text{ km (radius distance of point of re-entry)}$$

and

$$r_{Es} \cong r_{EM} - 0.87 r_{EM} \left(\frac{M_M}{M_E} \right)^{2/5}$$

Using the conservation of angular momentum and the definition of C_{3E} ,

$$r_r V_r \cos \Gamma_r = r_{ca} V_{ca}$$

$$V_{ca}^2 = C_{3E} + \frac{2\mu_E}{r_{ca}}$$

$$V_r^2 = C_{3E} + \frac{2\mu_E}{r_r}$$

then

$$r_r^2 V_r^2 \cos^2 \Gamma_r = r_{ca}^2 V_{ca}^2$$

$$r_r^2 \left(C_{3E} + \frac{2\mu_E}{r_r} \right) \cos^2 \Gamma_r = r_{ca}^2 \left(C_{3E} + \frac{2\mu_E}{r_{ca}} \right)$$

$$r_{ca}^2 (C_{3E}) + r_{ca} (2\mu_E) - r_r^2 \cos^2 \Gamma_r \left(C_{3E} + \frac{2\mu_E}{r_r} \right) = 0$$

$$r_{ca}^2 + \left(\frac{2\mu_E}{C_{3E}} \right) (r_{ca}) - \left(\frac{r_r^2 \cos^2 \Gamma_r}{C_{3E}} \right) \left(C_{3E} + \frac{2\mu_E}{r_r} \right) = 0$$

and

$$r_{ca} = -\frac{\mu_E}{C_{3E}} + \left[\frac{\mu_E^2}{C_{3E}^2} + \left(\frac{r_r^2 \cos^2 \Gamma_r}{C_{3E}} \right) \left(C_{3E} + \frac{2\mu_E}{r_r} \right) \right]^{1/2} \quad (1)$$

¹A detailed discussion of Tables 1 through 5 appears in Section IV-B.

Table 1. Selenocentric injection conditions and major-body angles

Launch date, March 1969	Lighting condition at injection	Visibility ^b from DSIF at injection	Selenocentric coordinates						Geocentric		Earth-Moon probe angle deg	Sun-Moon probe angle deg	Earth-Moon probe angle deg
			Time of injection GMT	Radius km	Velocity km/sec	Path angle deg	Azimuth angle deg	Lat. deg	Long. deg	Lat. deg			
8	Day	1	00 19 51	1,768	2,567	57.9	111.2	24.0	8.1	-15.6	40.4	62.2	46.9
9	Day	1	01 29 44	1,768	2,562	59.1	108.1	24.1	8.2	-21.1	36.1	73.7	60.3
10	Day	1	02 36 18	1,768	2,561	58.6	106.5	24.2	8.2	-25.4	33.7	85.3	73.9
11	Night	1	03 46 15	1,768	2,562	57.1	108.2	24.2	8.2	-28.0	31.4	96.9	87.6
12	Night	1	04 59 5	1,768	2,566	55.4	110.9	24.1	8.1	-28.6	29.1	108.5	101.5
13	Night	1	05 50 37	1,768	2,571	53.9	112.9	23.9	8.1	-27.1	31.8	119.7	115.2
14	Night	1	06 36 50	1,768	2,588	51.2	116.5	23.8	8.0	-23.8	35.1	130.6	128.9
15	Night	1	07 21 52	1,768	2,611	48.8	118.9	23.6	7.9	-19.0	37.6	140.9	142.5
16	Night	1	07 48 15	1,768	2,647	46.1	120.2	23.6	7.9	-13.2	43.7	149.6	155.8
20	Night	2	19 05 00	1,768	2,606	54.4	118.5	23.7	8.0	14.8	283.8	138.7	151.8
21	Night	2	19 59 15	1,768	2,604	55.0	122.1	23.6	7.9	19.8	281.9	128.3	136.3
22	Night	2	20 51 30	1,768	2,605	55.9	123.1	23.5	7.8	24.0	280.8	117.2	124.5
23	Night	2	21 47 17	1,768	2,604	56.9	124.2	23.4	7.8	27.0	279.3	105.8	113.0
24	Night	2	22 36 01	1,768	2,602	58.1	124.1	23.4	7.8	28.6	279.9	94.3	101.7
25	Day	2	23 27 33	1,768	2,599	59.6	122.8	22.9	7.8	28.8	280.0	82.7	90.5
27	Day	2	00 18 50	1,768	2,595	61.0	120.3	23.2	7.8	27.5	280.0	71.1	79.2
28	Day	2	01 13 00	1,768	2,598	61.8	116.4	23.4	7.9	24.9	281.0	59.6	71.3
29	Day	2	02 00 30	1,768	2,603	62.2	114.1	23.6	8.0	21.1	282.7	48.8	61.3
30	Day	2	02 44 30	1,768	2,617	61.7	106.0	23.8	8.1	16.2	286.5	38.8	50.5

^aFor launch dates of March 8 through March 16, the landing site will be San Antonio, Texas; for March 20 through 30, the landing site will be Bourke, Australia.^bNumbers denote the following tracking stations:

1. Johannesburg, South Africa
2. Goldstone, California

Table 2. Characteristics of the selenocentric hyperbola

Launch date ^a March 1969	Semi-transverse axis km/sec	Eccentricity	Inclination ^b deg	Longitude of the ascending node deg	Argument of perigee deg	Closest approach distance km	Energy C_{3AR} km ² /sec ²	Angular momentum C_1 km ² /sec
8	-4,623.1	1.121	38.8	304.9	344.3	560.7	1.060	2,414.2
9	-4,714.0	1.117	42.7	318.0	345.6	551.0	1.040	2,390.9
10	-4,780.4	1.120	45.6	328.4	351.6	574.0	1.025	2,442.1
11	-4,765.5	1.127	48.1	336.2	0.7	607.5	1.028	2,516.7
12	-4,704.7	1.139	50.5	342.2	12.1	653.8	1.042	2,617.9
13	-4,543.7	1.157	53.1	347.3	24.8	713.9	1.079	2,747.3
14	-4,240.8	1.186	55.8	352.9	38.3	790.4	1.156	2,910.1
15	-3,804.1	1.230	57.9	359.7	51.7	875.8	1.288	3,093.8
16	-3,310.9	1.292	58.5	8.1	64.6	968.4	1.480	3,298.5
20	-3,837.6	1.178	44.5	50.9	67.6	684.9	1.277	2,704.1
21	-3,903.7	1.172	44.1	59.1	71.8	671.5	1.255	2,673.5
22	-3,908.9	1.167	41.9	68.8	74.4	654.4	1.254	2,636.4
23	-3,925.2	1.160	38.1	79.6	75.0	628.1	1.249	2,578.5
24	-3,967.4	1.149	33.0	91.7	73.0	591.8	1.235	2,496.7
25	-4,023.9	1.135	26.2	105.0	68.9	543.1	1.218	2,383.8
27	-4,021.7	1.125	19.7	125.2	58.0	502.4	1.219	2,287.4
28	-3,991.8	1.117	12.6	158.0	35.0	468.6	1.228	2,205.1
29	-3,873.9	1.118	10.4	220.6	344.2	457.2	1.265	2,178.5
30	-3,614.3	1.132	16.3	266.9	312.6	477.1	1.356	2,232.7

^aFor launch dates of March 8 through March 16, the landing site will be San Antonio, Texas; for March 20 through 30, the landing site will be Bourke, Australia.^bRelative to the Earth's equatorial plane.

Table 3. Characteristics of the point of exit from the lunar sphere of influence

Launch date - March 1969	Time from launch hr	Distance from Moon km	Distance from Earth km	Selenocentric inertial coordinates ^a				Selenographic coordinates				Earth-Moon-probe angle deg	Sun-Moon-probe angle deg	Earth-Moon-probe angle deg
				Declination deg	Right ascension deg	Velocity km/sec	Path angle deg	Azimuth deg	Lat. deg	Long. deg	Velocity km/sec	Path angle deg	Azimuth deg	
8	12.2	56,122	336,481	26.2	86.8	1.114	88.3	129.4	4.3	41.8	1.121	83.6	260.0	44.1
9	12.2	55,816	334,541	27.6	103.1	1.106	88.3	133.4	6.2	42.5	1.112	83.6	260.5	43.9
10	12.2	55,582	333,566	25.9	119.9	1.099	88.2	137.8	6.5	44.0	1.105	83.7	260.4	44.4
11	12.2	55,418	332,741	21.4	135.4	1.101	88.2	142.3	5.4	45.2	1.107	83.8	260.0	44.5
12	12.1	55,332	332,342	14.7	149.5	1.107	88.1	146.4	3.0	46.2	1.113	83.8	259.2	44.6
13	12.0	55,339	332,584	6.6	162.2	1.123	88.0	149.6	-0.4	47.2	1.129	83.9	258.1	44.8
14	11.7	55,458	333,748	-2.4	174.4	1.157	87.9	151.8	-4.3	48.2	1.162	84.2	256.7	45.3
15	11.3	55,710	335,862	-11.2	186.7	1.212	87.8	152.5	-7.9	49.5	1.217	84.5	255.1	46.1
16	10.8	56,083	339,192	-19.0	200.2	1.288	87.8	151.0	-10.4	51.6	1.292	85.0	253.5	47.5
20	12.0	58,788	348,331	-22.7	255.8	1.208	88.2	139.5	-1.4	43.5	1.215	83.8	258.2	37.7
21	12.2	59,438	350,998	-25.5	268.3	1.199	88.2	137.9	-3.6	41.2	1.206	83.6	258.2	36.1
22	12.4	59,971	353,508	-26.1	281.6	1.198	88.2	135.0	-4.6	39.5	1.206	83.4	258.2	35.3
23	12.5	60,349	355,399	-24.6	295.0	1.196	88.3	131.6	-4.6	38.0	1.204	83.3	258.4	35.0
24	12.6	60,538	356,441	-21.2	308.0	1.190	88.3	128.2	-3.6	36.7	1.198	83.2	258.8	35.1
25	12.6	60,518	356,586	-16.1	320.5	1.182	88.4	124.1	-1.7	35.8	1.191	83.1	259.6	35.7
27	12.6	60,289	355,831	-9.5	332.4	1.182	88.4	121.5	1.0	35.2	1.191	83.1	259.9	36.8
28	12.4	59,872	354,699	-1.6	344.3	1.186	88.5	117.1	4.3	35.5	1.194	83.2	260.6	38.8
29	12.2	59,302	353,392	7.1	356.7	1.200	88.5	111.7	7.8	36.9	1.208	83.5	261.1	41.6
30	11.7	58,600	352,033	15.7	10.1	1.237	88.5	106.0	10.8	39.3	1.243	84.0	261.5	45.0

^aFor launch dates of March 8 through March 16, the landing site will be San Antonio, Texas, for March 20 through 30, the landing site will be Bourke, Australia.
^bRelative to the Earth's equatorial plane.

Table 4. Characteristics of the geocentric ellipse

Launch date, ^a March 1969	Semi-major axis km	Eccentricity	Inclination to equator deg	Longitude of the ascending node deg	Argument of perigee deg	Closest approach distance km	Energy C_{3x} km^2/sec^2	Angular momentum C_1 km^2/sec
8	242,222	0.973	46.4	15.8	15.1	6,428	-1.646	71,108.1
9	237,244	0.973	34.3	11.0	33.0	6,426	-1.680	71,090.6
10	231,168	0.972	30.0	5.5	52.3	6,426	-1.724	71,076.9
11	227,802	0.972	29.5	7.6	65.3	6,426	-1.750	71,069.3
12	226,028	0.972	29.7	20.8	68.6	6,428	-1.764	71,071.9
13	226,303	0.972	29.5	45.1	61.7	6,427	-1.761	71,070.4
14	228,749	0.972	31.1	79.2	45.1	6,428	-1.742	71,079.2
15	234,033	0.973	38.5	115.7	25.0	6,428	-1.703	71,090.6
16	240,581	0.973	55.6	145.9	9.2	6,428	-1.657	71,107.0
20	277,105	0.977	53.5	17.3	191.0	6,429	-1.438	71,174.7
21	287,046	0.978	39.0	14.6	205.1	6,428	-1.389	71,183.4
22	296,838	0.978	32.4	9.3	221.8	6,427	-1.343	71,193.4
23	304,656	0.979	30.3	6.7	236.4	6,427	-1.308	71,201.3
24	309,592	0.979	30.1	11.2	244.6	6,426	-1.287	71,204.6
25	311,044	0.979	30.1	24.1	245.5	6,426	-1.281	71,205.8
27	311,920	0.979	30.2	45.6	238.7	6,426	-1.278	71,206.1
28	306,687	0.979	31.7	74.0	225.2	6,427	-1.300	71,202.4
29	297,709	0.978	37.2	105.2	208.7	6,429	-1.339	71,201.1
30	288,285	0.978	49.3	133.7	194.0	6,428	-1.383	71,187.5

^aFor launch dates of March 8 through March 16, the landing site will be San Antonio, Texas; for March 20 through 30, the landing site will be Bourke, Australia.

Table 5. Characteristics of the points of re-entry and impact

Launch date * March 1969	Lighting at re-entry	Date of re-entry March 1969	Time of re-entry GMT hr min sec	Radius km	Earth-fixed coordinates						Inertial coordinates				Earth-Moon distance km	Impact azimuth deg
					Lat. deg	Long. deg	Velocity km/sec	Path angle deg	Azimuth deg	Declination deg	Right ascension deg	Velocity km/sec	Path angle deg	Azimuth deg		
8	Day	10	22 17 51	6,500	1.8	233.5	10.679	-6.0	42.0	1.8	16.4	11.000	-5.8	43.9	370,653	52.4
9	Day	11	23 27 44	6,500	11.5	225.6	10.608	-6.0	57.2	11.5	27.0	10.998	-5.8	58.5	369,744	71.6
10	Day	13	00 34 13	6,500	19.0	220.5	10.585	-6.3	67.3	19.0	39.6	10.997	-6.1	68.2	369,397	84.4
11	Day	14	01 44 21	6,500	218.9	218.9	10.590	-5.7	68.1	22.6	56.5	10.996	-5.5	69.0	369,725	88.3
12	Day	15	02 57 16	6,500	23.2	217.1	10.595	-5.4	66.8	23.2	73.9	10.995	-5.2	67.7	370,862	86.3
13	Night	16	03 48 46	6,500	22.5	219.5	10.587	-5.6	69.1	22.5	90.3	10.995	-5.3	70.0	372,872	89.6
14	Night	17	04 34 16	6,500	14.3	221.1	10.607	-7.7	58.2	14.3	104.2	10.996	-7.5	59.5	375,769	79.9
15	Night	18	05 19 20	6,500	6.5	226.6	10.640	-7.6	49.2	6.5	122.1	10.998	-7.4	50.8	379,477	64.3
16	Night	19	05 45 59	6,500	-2.8	239.0	10.744	-6.7	31.8	-2.8	142.1	10.999	-6.5	33.9	383,745	40.5
20	Night	23	16 57 30	6,500	3.2	113.3	10.672	-9.4	149.0	3.2	189.3	11.010	-9.2	145.8	401,600	146.2
21	Night	24	17 56 25	6,500	-7.6	106.4	10.618	-8.6	122.6	-7.6	197.5	11.012	-8.3	121.3	403,656	121.8
22	Night	25	18 48 30	6,500	-12.2	103.1	10.620	-9.2	121.1	-12.2	208.2	11.014	-8.8	119.9	404,337	120.1
23	Night	26	19 45 02	6,500	-19.7	103.7	10.611	-6.8	114.6	-19.7	224.0	11.016	-6.6	113.6	403,611	109.3
24	Night	27	20 33 32	6,500	-22.0	101.9	10.613	-7.5	112.4	-22.0	235.4	11.017	-7.3	111.6	401,536	109.7
25	Night	28	21 25 33	6,500	-24.3	104.3	10.609	-6.0	108.8	-24.3	251.8	11.017	-5.8	108.0	398,261	110.7
27	Night	29	22 17 17	6,500	-23.1	107.6	10.608	-4.7	110.3	-23.1	269.0	11.017	-4.5	109.5	394,056	106.2
28	Day	30	23 02 00	6,500	-18.8	111.3	10.624	-3.5	115.8	-18.8	288.0	11.016	-3.3	114.5	389,200	118.8
29	Day	31	23 44 50	6,500	-12.8	118.1	10.660	-2.3	124.0	-12.8	306.5	11.014	-2.1	122.2	384,300	133.7
30	Day	2 ^b	00 22 30	6,500	-4.7	126.5	10.742	-1.0	136.2	-4.7	325.3	11.012	-0.8	133.8	379,600	150.5

*For launch dates of March 8 through March 16, the landing site will be San Antonio, Texas; for March 20 through 30, the landing site will be Bourke, Australia.
^bApril 2, 1969.

Therefore,

$$r_{ca} = f_1(C_{3E}, \Gamma_r)$$

$$e = 1 - \frac{r_{ca}}{a}$$

and

$$\eta_{rp} = 2\pi - \eta_{r0}$$

where

$$\eta_{r0} = \cos^{-1} \left[\frac{r_{ca}(1+e)}{e r_r} - \frac{1}{e} \right], \quad \pi \leq \eta_{r0} \leq 2\pi \quad (2)$$

(re-entry always occurs before closest approach).

Therefore,

$$\eta_{rp} = f_2(C_{3E}, \Gamma_r)$$

and

$$\eta_{sp} = \cos^{-1} \left[\frac{b^2 + r_{Es} a}{r_{Es}(r_{ca} - a)} \right] \quad (3)$$

where

$$b^2 = r_{ca}(r_{ca} - 2a), \quad 0 \leq \eta_{sp} \leq \pi.$$

Therefore,

$$\eta_{sp} = f_3(r_M, C_{3E}, \Gamma_r)$$

and finally

$$\eta_{sr} = \eta_{sp} - \eta_{rp} \quad (4)$$

or

$$\eta_{sr} = f_4(r_M, C_{3E}, \Gamma_r).$$

Figure 3 presents η_{sr} vs. T_F and C_{3E} for a re-entry angle of -6.0 deg.

5. The declination and right ascension of the exit point s are within 1.5 deg of the Moon at launch as seen from the Earth. The angular diameter of the LSOI is about 17 deg as seen from the Earth (Fig. 1 is obviously not to scale).

B. Types of Lunar Return Ascent Trajectories

There are two basic types of lunar return ascent trajectories, the direct-ascent return and the parking-orbit return. The direct-ascent return consists of a continuous powered flight from liftoff to injection into the transfer orbit.* In the case of a multiple-stage lunar return vehicle, the direct-ascent return consists of consecutive powered flights separated by short coast periods or stag-

ing periods. Figure 4 presents the altitude vs. range profile of a direct-ascent return trajectory. Launch occurs at point A_0 and is followed by injection into the transfer orbit at point A_1 .

The parking-orbit return consists of two powered flight phases separated by a coasting phase which is usually longer than a staging period. Figure 4 presents the altitude vs. range profile of a parking-orbit return trajectory. Launch occurs at B_0 and is followed by the first powered flight, which places the return vehicle at point B_1 , injection into a low circular satellite orbit about the Moon. The return vehicle coasts in this orbit to a prescribed location, point B_2 , where ignition of the second powered flight occurs. The second powered flight places the return vehicle at point B_3 , injection into the transfer orbit to the Earth.

Reference 2 has shown that the parking-orbit technique is superior to the direct-ascent technique for Earth-to-Moon trajectories because of several specific geometrical properties of Earth-to-Moon trajectories. Investigations of similar geometrical properties for Moon-to-Earth trajectories show that superiority depends upon the mission objectives.

Three geometrical properties which strongly influence the choice between the two lunar return techniques are the available launch sites, outward radial directions, and launch azimuths. The launch site is dependent upon the mission objectives since any point upon the lunar surface may be a landing site for an Earth-to-Moon trajectory and hence, a launch site for a Moon-to-Earth trajectory. The outward radial direction is dependent upon the launch date, the re-entry angle, and the flight time, which are mission dependent. Once these three parameters are chosen, the outward radial direction and the injection energy are specified. The launch azimuth on the Moon is not restricted by the usual factors restricting launches from the Earth, since there is no life on the Moon and the atmosphere and spin rate are negligible factors. Consequently, depending upon mission objectives, a considerable amount of flexibility can exist in these three geometrical properties, in contrast to the Earth-to-Moon trajectories.

The importance of flexible launch sites, outward radial directions, and launch azimuths is shown in Fig. 5, 6, and 7. Figure 5 presents the launch geometry of a typical lunar return trajectory for a particular launch day, re-entry angle, and flight time. The outward radial direction S and the injection energy are uniquely defined. Furthermore, the direction of closest approach P is defined

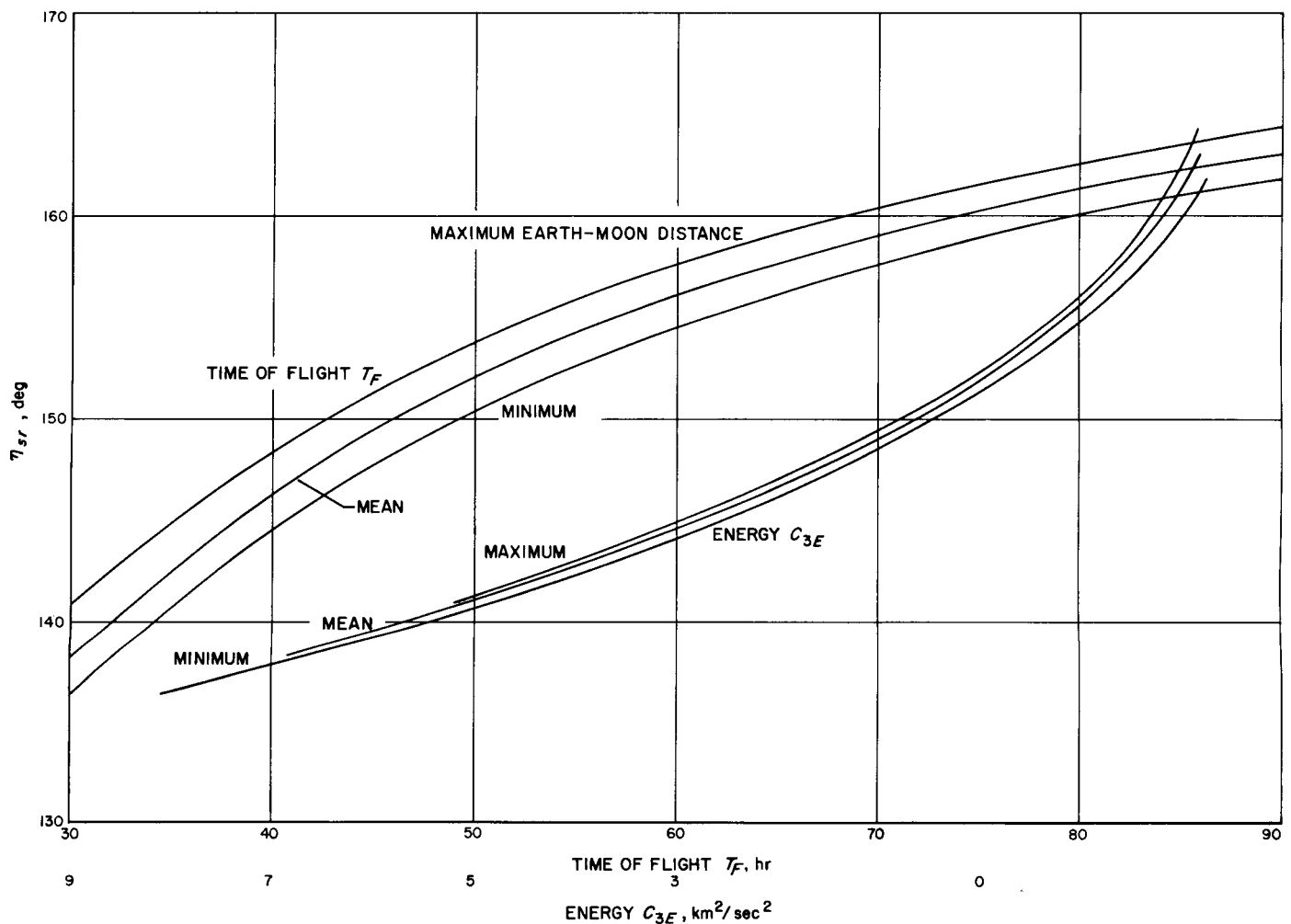


Fig. 3. In-plane angle between exit point and re-entry point vs. time of flight and energy C_{3E}

relative to S by an angle θ_s , where θ_s is a function of the closest approach distance to the Moon and the injection energy C_{3M} . The injection energy C_{3M} , like C_{3E} , is a function of the Earth-to-Moon distance, the flight time, and the re-entry angle. The closest approach distance depends upon the burnout radius distance and the burnout flight path angle.

From Fig. 1 and Ref. 1

$$C_{3M} \triangleq V_{PM}^2 - \frac{2\mu_M}{r_{Ms}}$$

and

$$a = -\frac{\mu_M}{C_{3M}}$$

where

$$\mu_M \triangleq G M_M. \quad (5)$$

The injection energy C_{3M} is constant for a fixed launch day, re-entry angle, and flight time. Furthermore,

$$e = 1 - \frac{r_{ca}}{a} \quad (6)$$

and

$$\theta_s = \cos^{-1} \left(-\frac{1}{e} \right). \quad (7)$$

From Eq. 5,

$$C_{3M} = V_b^2 - \frac{2\mu_M}{r_b}$$

and since C_{3M} is constant,

$$V_b = \left[C_{3M} + \frac{2\mu_M}{r_b} \right]^{1/2}. \quad (8)$$

Using the conservation of angular momentum and the definition of C_{3M} ,

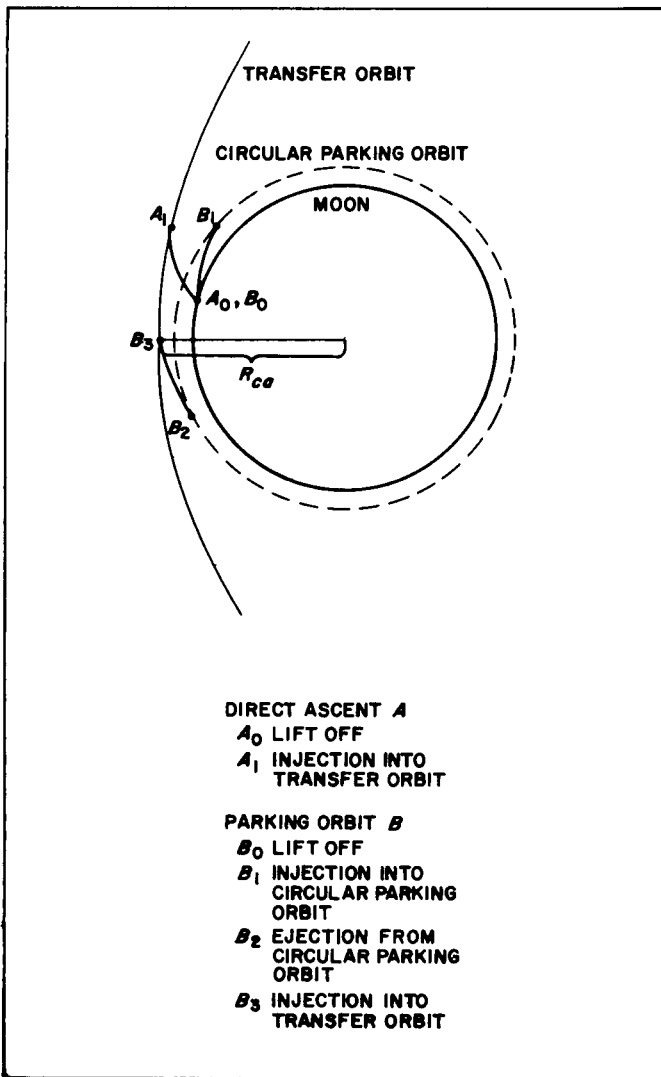


Fig. 4. Types of lunar return trajectories

$$r_{ca} V_{ca} = r_b V_b \cos \Gamma_b$$

$$C_{3M} = V_{ca}^2 - \frac{2\mu_M}{r_{ca}}$$

$$V_{ca} = \frac{r_b V_b \cos \Gamma_b}{r_{ca}}$$

$$V_{ca}^2 = C_{3M} + \frac{2\mu_M}{r_{ca}}$$

From Eq. (9) and Eq. (10)

$$\frac{(r_b V_b \cos \Gamma_b)^2}{r_{ca}^2} = C_{3M} + \frac{2\mu_M}{r_{ca}}$$

$$(r_b V_b \cos \Gamma_b)^2 = C_{3M} r_{ca}^2 + 2\mu_M r_{ca}$$

$$r_{ca}^2 + \frac{2\mu_M}{C_{3M}} r_{ca} - \frac{(r_b V_b \cos \Gamma_b)^2}{C_{3M}} = 0$$

$$r_{ca} = -\frac{\mu_M}{C_{3M}} + \left[\frac{\mu_M^2}{C_{3M}^2} + \frac{(r_b V_b \cos \Gamma_b)^2}{C_{3M}} \right]^{1/2}$$

and

$$r_{ca} = -\frac{\mu_M}{C_{3M}} + \left[\frac{\mu_M^2}{C_{3M}^2} + \left(\frac{r_b^2 \cos^2 \Gamma_b}{C_{3M}} \right) \left(C_{3M} + \frac{2\mu_M}{r_b} \right) \right]^{1/2}. \quad (11)$$

Assuming that optimum flight is desired for a given boost vehicle, injection occurs at the closest approach distance of the selenocentric hyperbola. The powered flight characteristics of importance here are the burning arc η_{lb} required to achieve the injection energy C_{3M} and the resulting burnout radius distance r_b . Since injection occurs at the closest approach distance, $\Gamma_b = 0$ and $r_{ca} = r_b$. Figure 6 presents the variation of θ_s with flight time T_F and injection energy C_{3M} for a closest approach distance of 1,768.6 km. Figure 5 shows that the sum of θ_s and η_{lb} forms an angle η_{ls} between the launch site vector \mathbf{R}_l and the outward radial direction \mathbf{S} in the trajectory plane which is defined by the outward radial direction, the injection point (point of closest approach), and the launch site. For a flight time of 70 hr, a re-entry angle of -6.0 deg, and a mean Earth-to-Moon distance, Fig. 6 shows that θ_s is equal to 134 deg for an assumed burnout

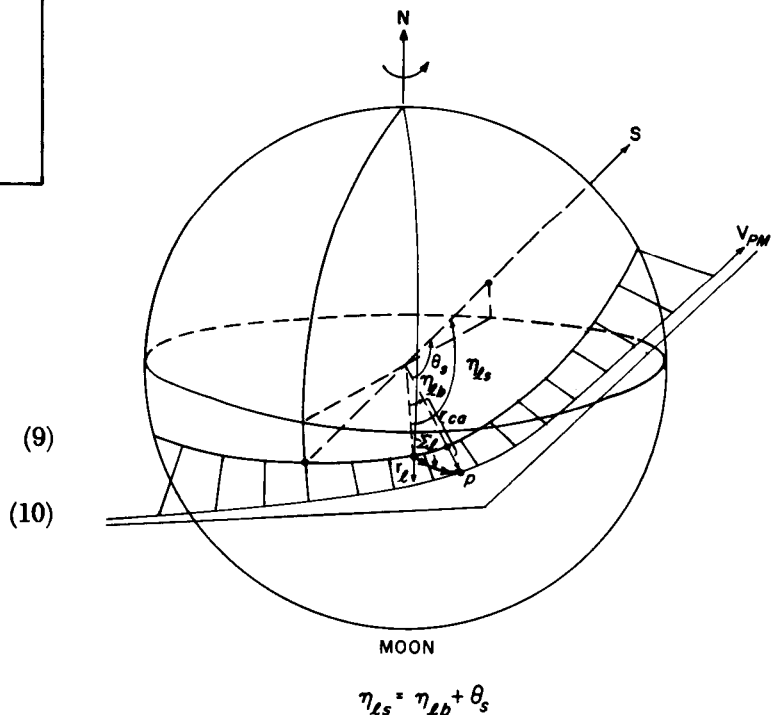


Fig. 5. Launch site location referenced to the outward radial direction

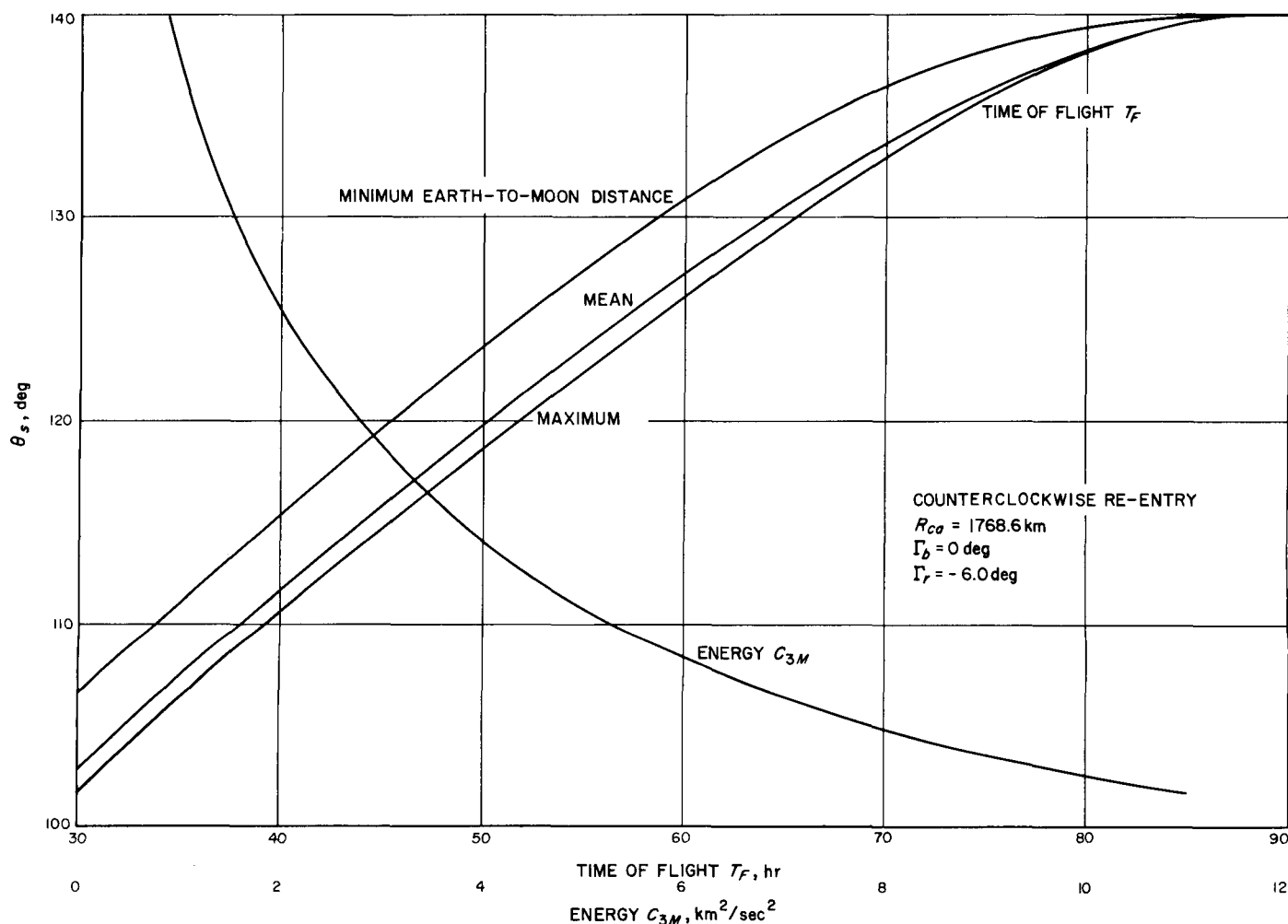


Fig. 6. Angle between outward radial direction and perisene vs. time of flight and energy C_{3M}

radius, r_b , of 1,768.6 km. Assuming that the boost vehicle requires a burning arc, η_{lb} , of 8.0 deg to achieve the required C_{3M} , η_{ls} results in a value of 142 deg. Using this value of η_{ls} , the locus of possible launch sites for a direct-ascent trajectory is obtained by rotating \mathbf{R}_l about \mathbf{S} at an angle η_{ls} of 142 deg. This locus is presented in Fig. 7. Each point in the locus represents a possible launch site. Associated with each point are a unique launch azimuth and a unique orbit inclination. If the mission objectives require launch sites other than those described by this locus, then non-optimum powered flight must occur. A certain amount of variation in the locus of launch sites may be obtained by varying flight time and therefore varying η_{ls} . However, mission constraints usually require a relatively fixed flight time.

Launch sites located within the circular locus require very inefficient direct-ascent powered flights since injection

occurs before the closest approach distance of the selenocentric hyperbola. These launch sites could best be utilized in the parking-orbit technique.

Launch sites located outside the circular locus require inefficient direct-ascent powered flights to a lesser extent. Equations 5 and 11 show that r_{ca} is a function of r_b and Γ_b . For a given lunar return boost vehicle, the burnout radius r_b and the burning arc η_{lb} vary little with variations in pitch control. Therefore, r_{ca} is essentially a function of burnout flight path angle Γ_b . If burnout occurs at an angle Γ_b , η_{ls} is no longer the sum of θ_s and η_{lb} but instead the sum of θ_s and η_{lb} minus the true anomaly angle η_{pb} where

$$\eta_{pb} = \cos^{-1} \left[\frac{b^2 + r_b a}{r_b (r_{ca} - a)} \right]$$

and

$$b^2 = r_{ca} (r_{ca} - 2a).$$

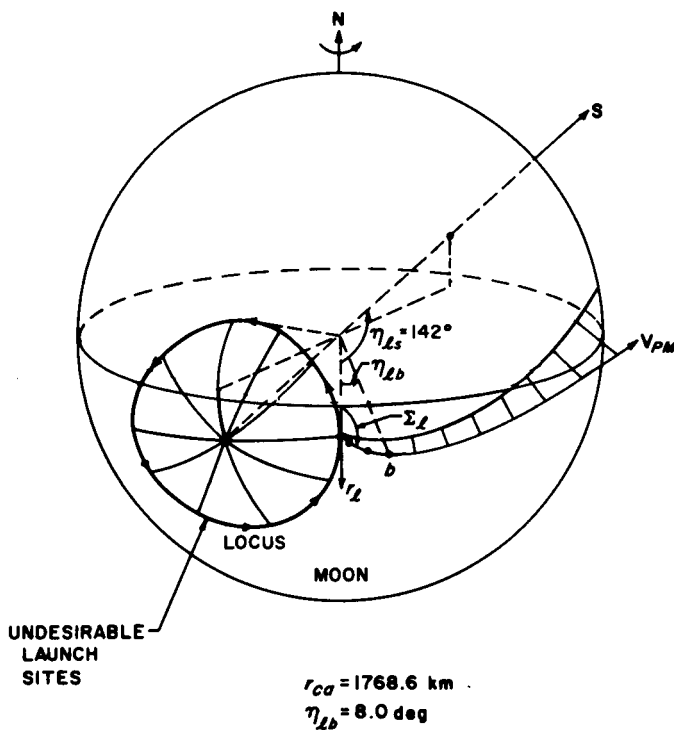


Fig. 7. Locus of launch sites for injection at closest approach distance

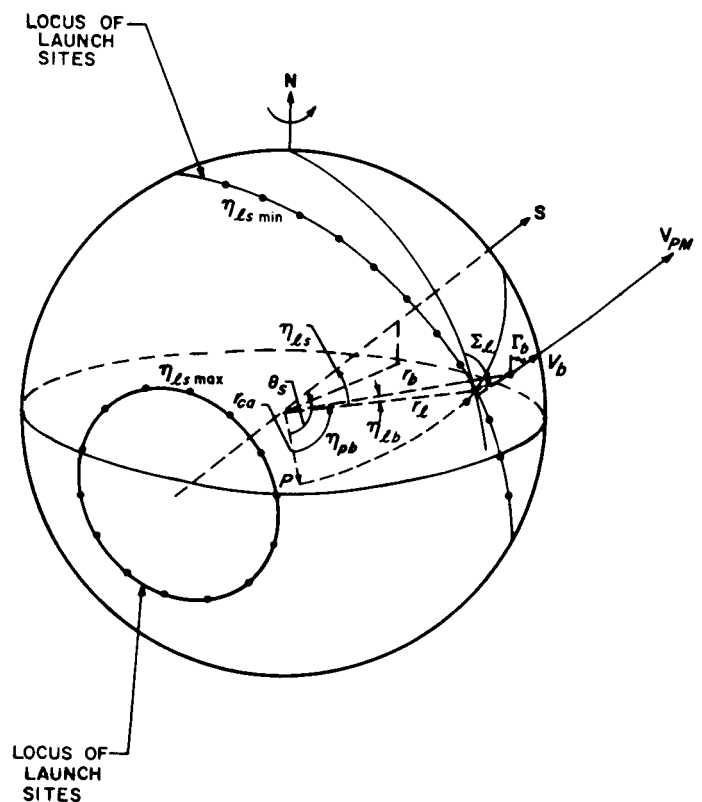


Fig. 8. Locus of launch sites for injection at positive Γ_b

Figure 8 presents the geometry and a typical locus of launch sites.

There is an extreme set of r_b and Γ_b which achieves the required C_{3M} for a given lunar boost vehicle using a direct-ascent trajectory. The extreme combination places a minimum value that may be obtained for η_{Ls} . The maximum value of η_{Ls} will be determined by trajectories that inject at the closest approach distance. As a result, a region of launch sites is defined such that $\eta_{Ls(\min)} \leq \eta_{Ls} \leq \eta_{Ls(\max)}$ for a given flight time as shown in Fig. 8. Launch sites located outside this region are best utilized by using the parking-orbit technique.

The previous discussion shows that the direct-ascent return trajectory is feasible depending upon the over-all mission objectives. The direct-ascent technique requires much simpler guidance and propulsion hardware, simplifies tracking and communication, and is more reliable. For this reason and the fact that the near-Earth trajectory is independent of the ascent trajectory, this Report

assumes a direct-ascent trajectory rather than a parking-orbit trajectory.

C. Rendezvous Return

A special class of the parking-orbit return trajectory of particular interest is the rendezvous return trajectory. In this type of trajectory, the return vehicle is launched in such a manner that a rendezvous with another vehicle or spacecraft is made at parking-orbit injection. The two vehicles combine during the coast and are then accelerated together into the transfer orbit to the Earth. The rendezvous return trajectory is restricted, compared with the general parking-orbit trajectory, in that a particular parking orbit must be used as well as a set of particular launch times. The parking orbit must be that of the orbiting vehicle and the launch time must be such that the sum of launch time and time of powered flight must equal times of injection at which the position of the orbiting vehicle corresponds to the point of injection into the parking orbit.

III. TRAJECTORY-COMPUTING TECHNIQUES

The Analytic Lunar Return Program and the Space Trajectories Program permit the design of a set of lunar return trajectories for a specified mission. The technique for trimming or searching-in this set of trajectories is based upon a specific set of search parameters.

A. Analytic Lunar Return Program

The Analytic Lunar Return Program is a joined conic program. The lunar return trajectory is split into two phases, near-Moon and near-Earth, as shown in Fig. 1. The near-Moon or selenocentric phase initiates upon the surface of the spherical Moon and terminates at the exit point of the LSOI. The near-Earth or geocentric phase initiates at the exit point of the LSOI and terminates at the impact point upon the spherical Earth. The selenocentric phase consists of a simplified powered flight followed by free flight in a hyperbolic orbit. The powered flight portion is simulated by specifying a launch site, a burning arc, and a burnout altitude. The geocentric phase consists of an elliptical or hyperbolic orbit terminating at the re-entry point, followed by a simplified re-entry trajectory described by a re-entry altitude, a maneuver angle, a maneuver time, and an impact site.

The basic input data consist of the selenographic longitude and latitude of the launch site, the launch date, the lunar powered-flight angle from launch to lunar burnout, the burnout altitude, the re-entry maneuver angle and maneuver time to impact, the longitude and latitude of the impact site, the re-entry angle, the re-entry altitude, and the total time of flight. The output data consist of spherical position and velocity parameters and conic characteristics at selenocentric injection, at geocentric re-entry, and at geocentric impact. A more detailed description of this program appears in Ref. 3.

The objective of this program is twofold. First, the simplicity of the program permits rapid computation of many trajectories and, therefore, permits a parametric study of all trajectories of interest. Second, once the ideal set of trajectories has been obtained from the parametric study, good initial conditions are available as input to the more accurate Space Trajectories Program.

B. Space Trajectories Program

The Space Trajectories Program computes the motion of a probe confined to the solar system and influenced

by the nonspherical Earth and Moon, and point masses representing the Sun, Venus, Mars, and Jupiter. Any of these bodies may serve as the reference body at the injection epoch. Stepwise numerical integration of the equations of motion appropriate to either a Cowell or an Encke scheme serves to step the probe along its flight to one of the previously mentioned bodies, which then serves as a target.

The starting conditions may be entered in cartesian or spherical coordinates based on one of four reference frames: mean equator and equinox of 1950.0, mean ecliptic and equinox of 1950.0, true equator and equinox of date, and true ecliptic and equinox of date. In addition, the Earth-fixed spherical set of starting conditions, based upon a rotating Earth, is available for the Earth as the injection body, and the selenographic or Moon-fixed spherical set of starting conditions, based upon a rotating Moon, is available for the Moon as the injection body. The output data may consist of any of the above quantities, ephemeris information expressed in any one of the cartesian or spherical coordinate systems, elements of the osculating two-body orbit referred to one of the standard cartesian systems, geometrical angles between the probe and the celestial bodies, and tracking characteristics from a maximum of 15 tracking stations.

The Space Trajectories Program is basically a free-flight program. A simplified powered-flight trajectory may be simulated which assumes a constant-thrust constant-burning-rate motor with thrust direction fixed in space. In addition, a simplified re-entry trajectory may be simulated as an arc that connects the re-entry point with the impact point, lies in the orbit plane, and has a re-entry radius of r_r , a maneuver angle of η_r , and a maneuver time of t_r . A more detailed description of this program appears in Ref. 4 and 5.

C. Search Parameters

The search parameters for a lunar return trajectory are governed by the set of terminal conditions that must be satisfied. Such a set consists of a particular re-entry angle Γ_r and an impact site defined by a latitude ϕ_i and a longitude θ_i . From these three desired terminal conditions and the general trajectory constants such as the re-entry radius, maneuver angle, etc., a set of desired search parameters can be computed which varies with burnout conditions in a fairly linear fashion. This set is

based upon the impact parameter \mathbf{B} and consists of $\mathbf{B} \cdot \mathbf{T}$, $\mathbf{B} \cdot \mathbf{R}$, T_F , and θ_{ca} .*

Since the near-Earth orbit for a lunar return trajectory is either elliptic or hyperbolic depending upon the flight time, two definitions of the impact parameter and of the orthogonal vectors \mathbf{R} , \mathbf{S} , \mathbf{T} are required. First, for the elliptical case, the impact parameter \mathbf{B} is defined as the position vector in the plane of the trajectory, originating at the center of gravity of the target body and directed normally to the perigee direction of the ellipse. Vector \mathbf{S} is a unit vector in the direction of perigee \mathbf{P} ; \mathbf{T} is a unit vector perpendicular to \mathbf{S} that lies in the equatorial plane as shown in Fig. 9; \mathbf{R} is a unit vector which forms the third vector of the dextral orthogonal system \mathbf{R} , \mathbf{S} , \mathbf{T} . Second, for the hyperbolic case, the impact parameter \mathbf{B} is defined as the position vector in the plane of the trajectory, originating at the center of gravity of the target body and directed normally to the incoming asymptote of the hyperbola. Vector \mathbf{S} is a unit vector in the direction of the incoming asymptote; \mathbf{T} is a unit vector perpendicular to \mathbf{S} that lies in the equatorial plane as shown

in Fig. 9; and \mathbf{R} is a unit vector that forms the third vector of the dextral orthogonal system \mathbf{R} , \mathbf{S} , \mathbf{T} . In both cases, \mathbf{B} is approximately the vector miss which would occur if the target body had no mass. The search parameters, $\mathbf{B} \cdot \mathbf{T}$ and $\mathbf{B} \cdot \mathbf{R}$, are the projections of the impact parameter \mathbf{B} upon the vectors \mathbf{T} and \mathbf{R} , respectively.

The time of flight T_F and the longitude of closest approach θ_{ca} complete the set of search parameters; T_F , $\mathbf{B} \cdot \mathbf{T}$, and $\mathbf{B} \cdot \mathbf{R}$ determine the shape of the trajectory, whereas θ_{ca} determines the launch time. The search parameters $\mathbf{B} \cdot \mathbf{T}$, $\mathbf{B} \cdot \mathbf{R}$, and T_F are very powerful in searching in a set of trajectories because of their linear behavior with variations in lunar burnout conditions. Figures 1 and 9 show that a perturbation of any one of the lunar burnout conditions causes direct variations in both the flight time and the impact parameter in a continuous functional manner.

The longitude of closest approach, θ_{ca} , is used to control launch time for two reasons; first, it exists for all trajectories, and second, it is directly dependent upon launch time when $\mathbf{B} \cdot \mathbf{T}$, $\mathbf{B} \cdot \mathbf{R}$, and T_F are held constant. References 5 and 6 present a detailed discussion of the equations and characteristics of the search parameters $\mathbf{B} \cdot \mathbf{T}$, $\mathbf{B} \cdot \mathbf{R}$, T_F , and θ_{ca} .

D. Search Technique

The search procedure consists of computing an initial trajectory based upon the selenocentric initial conditions obtained from the Analytic Lunar Return Program, and then computing three perturbed trajectories. The three perturbed trajectories are obtained by independently incrementing three of the initial set of starting conditions. The size of the increments depends upon the linearity of the perturbed initial conditions with the search parameters. The variations of the search parameters are associated with the corresponding perturbations through a linearized differential correction scheme, and corrections to the initial set of starting conditions are made. This process is repeated until the desired search parameters are obtained within specified convergence criteria. An adjustment is then made upon launch time and the entire process is repeated.

At the present time, the Space Trajectories Program is incapable of computing a lunar-boost powered-flight trajectory. As a result, the versatility of the lunar return search program is restricted and the computation of a set of realistic burnout or injection conditions is impossible since the injection conditions of a launch-to-impact

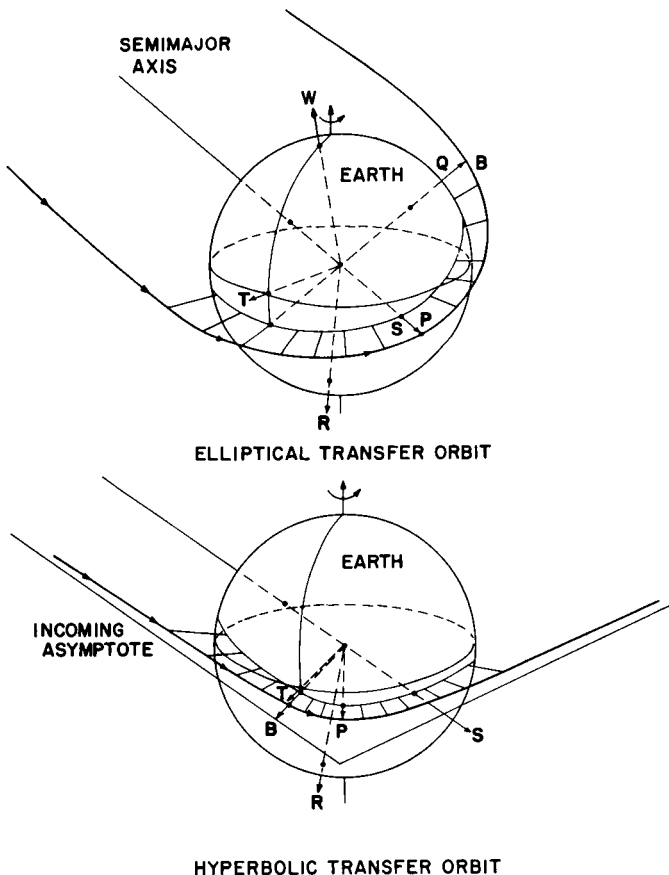


Fig. 9. Definition of the impact parameter \mathbf{B}

trajectory are dependent upon the launch vehicle characteristics. For this reason, the trajectories described in this Report begin at an approximate lunar injection point. However, a booster-powered flight program is presently being added to the Space Trajectories Program to eliminate this restriction.

Figure 10 presents the search logic using the present Space Trajectories Program. An initial trajectory is computed using injection conditions obtained from the Analytic Lunar Return Program. The initial trajectory is integrated to the point of closest approach to the Earth. At this point, the desired search parameters $B \cdot T$, $B \cdot R$, and T_F are computed using parameters from the initial trajectory along with the semimajor or semitransverse axis a , the closest approach distance r_{ca} , and the inclination i of the orbit plane to the equatorial plane, obtained from the Analytic Lunar Return Program solution. These desired search parameters are held constant throughout the first search loop. Three independent search variables, A , B , and C , which are obtained from the initial set of injection conditions, are then independently incremented and three perturbed trajectories are integrated to the point of closest approach to the Earth. The actual $B \cdot T$, $B \cdot R$, and T_F from the three perturbed and initial trajectories are compared with the desired $B \cdot T$, $B \cdot R$, and T_F . A linearized differential correction scheme computes the corrections to the selenographic independent variables required to cause these actual search parameters to approach the desired search parameters. The corrections are added to the unperturbed selenographic injection conditions and a corrected trajectory is integrated to the point of closest approach to the Earth. The resulting search parameters are tested according to the convergence criteria specified. If the test is negative, then this search loop is repeated. New values for the desired $B \cdot T$ and $B \cdot R$ are computed using parameters a , r_{ca} , and i from the corrected trajectory. If the test is affirmative, a test for convergence is made upon θ_{ca} . If this test is affirmative, the search is completed and the trajectory is printed. If this test is negative, a correction to the launch time, Δt , is made. Since the lunar powered-flight portion of the trajectory is not simulated, the correction to launch time is made indirectly by fixing the Moon-fixed spherical (selenographic) injection conditions and correcting the injection time by Δt . The selenographic injection conditions with the corrected injection time are integrated to

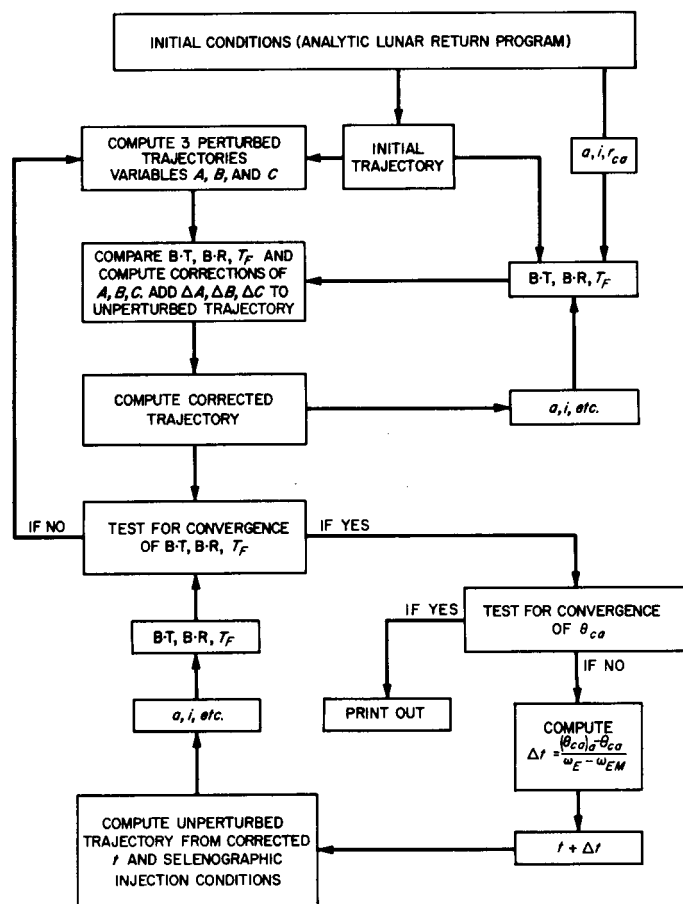


Fig. 10. Present search routine for Space Trajectories Program

the point of closest approach to the Earth. This trajectory now becomes the corrected trajectory for the search on $B \cdot T$, $B \cdot R$, and T_F . The desired search parameters are recomputed based upon this new corrected trajectory and the search loop is repeated. This entire procedure is repeated until all the convergence criteria are met. This search technique is known as a 3×3 search followed by a 1×1 search.

An analysis was made to determine the ideal set of three independent variables to use from the selenographic injection conditions. The results showed that azimuth, velocity, and flight-path angle composed the ideal set. Using this set in the above search technique, a typical set of lunar return trajectories was designed for the month of March, 1969.

IV. A TYPICAL SET OF LUNAR RETURN TRAJECTORIES

The design of a set of trajectories consists of the following steps: definition of the mission, design and programming of the required trajectory-computing programs, specification of the trajectory design constraints, determination of the set of best trajectories by means of a parametric analysis, and searching-in the best set of trajectories.

A typical set of lunar return trajectories is presented for the month of March, 1969. The mission is to return a spacecraft from the surface of the Moon to one of two landing sites upon the surface of the Earth. The required trajectory-computing programs designed and programmed for this mission are presented in Sections III-A and III-B. The trajectory design constraints are presented in Section IV-A. The parametric study that determined the best set of trajectories is not presented in this Report but the searched-in trajectories are presented in Section IV-B.

A. Design Constraints

The trajectory design constraints are chosen so that a manned lunar return trajectory is simulated from lunar burnout to geo-impact. The constraints are as follows:

<i>Parameters</i>	<i>Constraints</i>
Launch month	March 1969
Launch site (Moon)	Palus Putredinis
lat., deg	27.0
long. (east), deg	0.0
Powered-flight angle, deg	8
Time of powered flight, sec	25.0
Burnout radius distance, km	1,768.0
Flight time, hr	70.0
Re-entry	Counterclockwise
Re-entry radius distance, km	6,500
Re-entry flight path angle, deg	-6.0
Re-entry maneuver angle, deg	40.0
Time of re-entry maneuver, hr	0.2
Landing sites	
San Antonio, Texas	
lat., deg	29.48
long. (east), deg	261.0
Bourke, Australia	
lat., deg	-30.09
long. (east), deg	145.6

B. Trajectory Characteristics

The Analytic Lunar Return Program was used to investigate all the possible trajectories satisfying the constraints listed above. The results indicated that March 8 through 16 yielded acceptable trajectories for landing site No. 1 (San Antonio, Texas) and that March 20 through 25 and 27 through 30 yielded acceptable trajectories for landing site No. 2 (Bourke, Australia). The selenographic injection conditions from the analytic program were entered into the Space Trajectories Program for each of these days. Using the search technique described in Section III-D, integrated trajectories were obtained. Figure 1 shows the general characteristics of these trajectories.

1. Ascent Trajectory

The direct-ascent technique is used. Figures 11 and 12 show the lunar track of the ascent trajectories initiating at the launch site and terminating at the injection points for March 8 and 16 and for March 20 and 30, consecutively. Figure 1 shows that when the Moon is at positive declination at launch, the landing site for the type of trajectory required must have a negative latitude. Therefore, since the declination of the Moon is positive during the period of March 20 through 30, the landing site is Bourke, Australia, at a *negative* latitude of 30.09 deg. Similarly, the declination of the Moon is negative during the period of March 8 through 16; therefore, the landing site is San Antonio, Texas, at a *positive* latitude of 29.48 deg. As a result, Fig. 11 and 12 present lunar tracks for San Antonio landings and Bourke landings, consecutively. These figures show that, regardless of where the impact site is located upon the Earth, launchings must be made in the lunar-east direction for a direct-ascent trajectory. In addition, the injection points for the first and last days in each of the two launch periods are located close together, enabling direct tracking and communication during the ascent phase of flight throughout the launch periods.

Table 1 presents the following injection conditions: the lighting conditions, the visibility from the Deep Space Instrumentation Facility (DSIF), the Moon-fixed spherical coordinates, the selenocentric inertial velocity, the geocentric latitude and longitude, and the major-body angles. The lighting condition at injection is, in general, the same as the lighting condition at launch since the



Fig. 11. Lunar tracks of the ascent trajectories, impact site, San Antonio, Texas

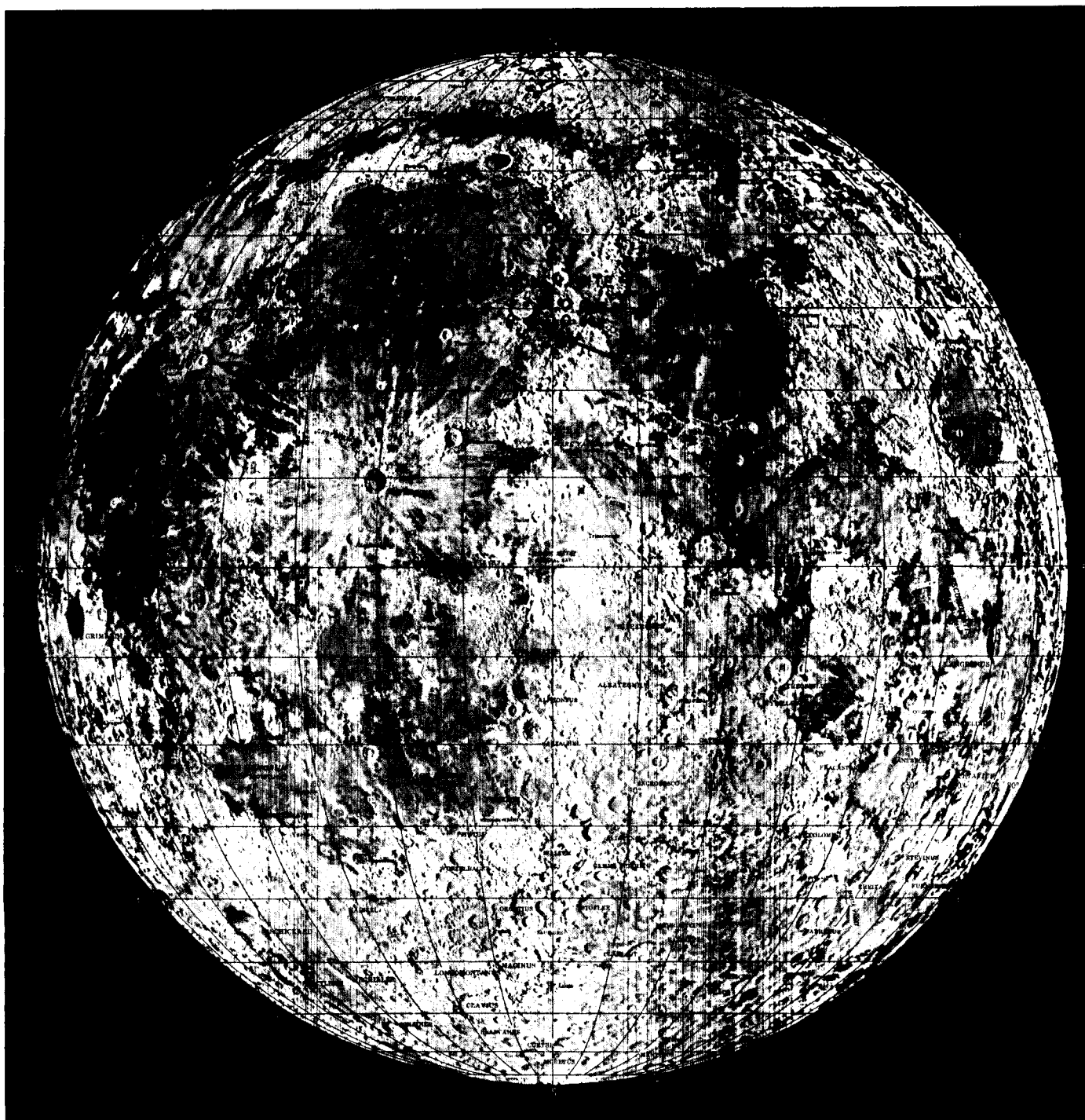


Fig. 12. Lunar tracks of the ascent trajectories, impact site, Bourke, Australia

powered-flight arc is only 8.0 deg. The lighting condition varies from month to month as a result of the changing relationship between the position of the Moon and the quarters of the month. The visibility from the DSIF is governed by the impact site. The San Antonio impact site is at positive latitude, which places the Moon at negative latitude at launch (as seen from the Earth) and hence, the DSIF station at Johannesburg, South Africa, or Woomera, Australia, in the southern hemisphere can observe the launch. The reverse is true for the Bourke impact site at a negative latitude; the DSIF station at Goldstone, California, can observe the launch. The launch period from March 20 through 30 has a launch day apparently missing, March 26. This apparent discontinuity is caused by the fact that fixing the impact site at Bourke and the flight time at 70 hr creates a geometrical situation which has no trajectory solution for this launch day. The path angle ranges in value from 45 to 60 deg, which indicates that this launch site (Palus Putredinis) is not optimum from the payload viewpoint. The path angle should be zero, injection at periselene.

2. Transfer Orbit

The transfer orbit is defined as that portion of the launch-to-impact trajectory which lies between the lunar injection point and the re-entry point into the Earth's atmosphere. Section II-A has shown that the transfer orbit can be expressed as two conics, a selenocentric hyperbola from the lunar injection point to the point of exit from the lunar sphere of influence and a geocentric ellipse having an eccentricity of at least 0.960 from the exit point to the re-entry point.

Table 2 presents the characteristics of the selenocentric hyperbola for each acceptable launch day in March, 1969. The conic characteristics are taken as the osculating conic characteristics at the time of selenocentric injection. Table 3 presents the characteristics of the point of exit from the LSOI. Table 4 presents the characteristics of the geocentric ellipse. The conic characteristics are taken as the osculating conic characteristics at the time of closest approach to the Earth. Figures 13 through 31 show the Earth tracks relative to the DSIF for the final day of flight for each acceptable launch day in March, 1969.

The dependence of periselene upon injection path angle when the injection radius distance is held fixed is evident from Tables 1 and 2. The variation of the energy C_{3M} with launch day for a fixed flight time and re-entry angle is a result of the varying Earth-to-Moon distance (taken at the time of re-entry). The minimum Earth-to-Moon distance occurs for the launch date March 10,

which exhibits the minimum value of C_{3M} . Table 3 shows the changing size of the LSOI according to the varying Earth-to-Moon distance. The time of transit from launch to exit from the LSOI is about 12 hr. The exit points occur at angles from the Earth-Moon line varying from 35 to 48 deg. From Table 4, eccentricities ranging from 0.972 to 0.979 and perigees ranging from 6,426 to 6,429 km characterize the geocentric ellipse.

Figures 13 through 31 show the variation of the Earth track for the last day of flight as a function of launch day. The reversal or looping of the Earth track is caused by the change in angular rate of the probe relative to the Earth. When the probe is at a large distance from the Earth (40,000 mi), it appears stationary in inertial space, similar to a star. Thus, as the Earth rotates under this apparently stationary object, an Earth track is made that appears as a fairly straight line parallel to the Earth's equator. However, as the probe nears the Earth, its angular rate relative to the Earth increases to a value greater than the angular rate of the Earth and, hence, causes the Earth track to change directions. The changing shape of the Earth tracks from launch day to launch day is a result of the changing declination of the Moon at launch. As the magnitude of the declination of the Moon increases, the inclination of the trajectory plane decreases, and as the magnitude of the declination of the Moon decreases, the inclination of the trajectory plane increases; see Tables 1 and 4 (the geocentric latitude of injection is approximately equal to the declination of the Moon at launch). The reversal of direction of the Earth track is a function of the inclination of the trajectory plane to the equatorial plane since the angular rate of the probe relative to the Earth is dependent upon inclination. The larger inclinations cause a looping, whereas the smaller inclinations cause just a reversal. The numbers on the Earth tracks are altitudes in statute miles and times before impact in hours (units desired by DSIF personnel). The solid line indicates that at least one of the three DSIF stations is able to track, whereas the dashed line indicates that none of the DSIF stations is able to track.

3. Re-entry Trajectory

The re-entry trajectory is defined as that portion of the launch-to-impact trajectory which lies between the re-entry point and the impact point. The design of the re-entry trajectory is a field of its own and is not considered in any detail during the design of the over-all lunar return trajectory. Therefore, the re-entry trajectory is assumed as any path that connects the re-entry point

with the impact point and has a re-entry radius of r_r , a re-entry flight path angle of Γ_r , a maneuver angle of η_r , and a maneuver time of t_r , and lies in the plane of the trajectory. Figure 1 shows a typical re-entry trajectory. The design of the trajectory-computing programs discussed in Section III-B and the discussion of the trajectory characteristics are based upon this assumption.

Table 5 presents the characteristics of the point of re-entry for each of the acceptable days in March, 1969. Three days in each of the two launch periods exist which have daylight launches and impacts, March 8 through 10 and March 28 through 30. The re-entry date of April 1 has no solution for reasons similar to those given for the missing March 26 launch date. The Earth-fixed and inertial velocities differ by about 0.32 km/sec for these counterclockwise trajectories. If clockwise trajectories are used, about 0.6 km/sec additional retrorocket capability is required. The time of impact is equal to the time of re-entry plus 0.2 hr.

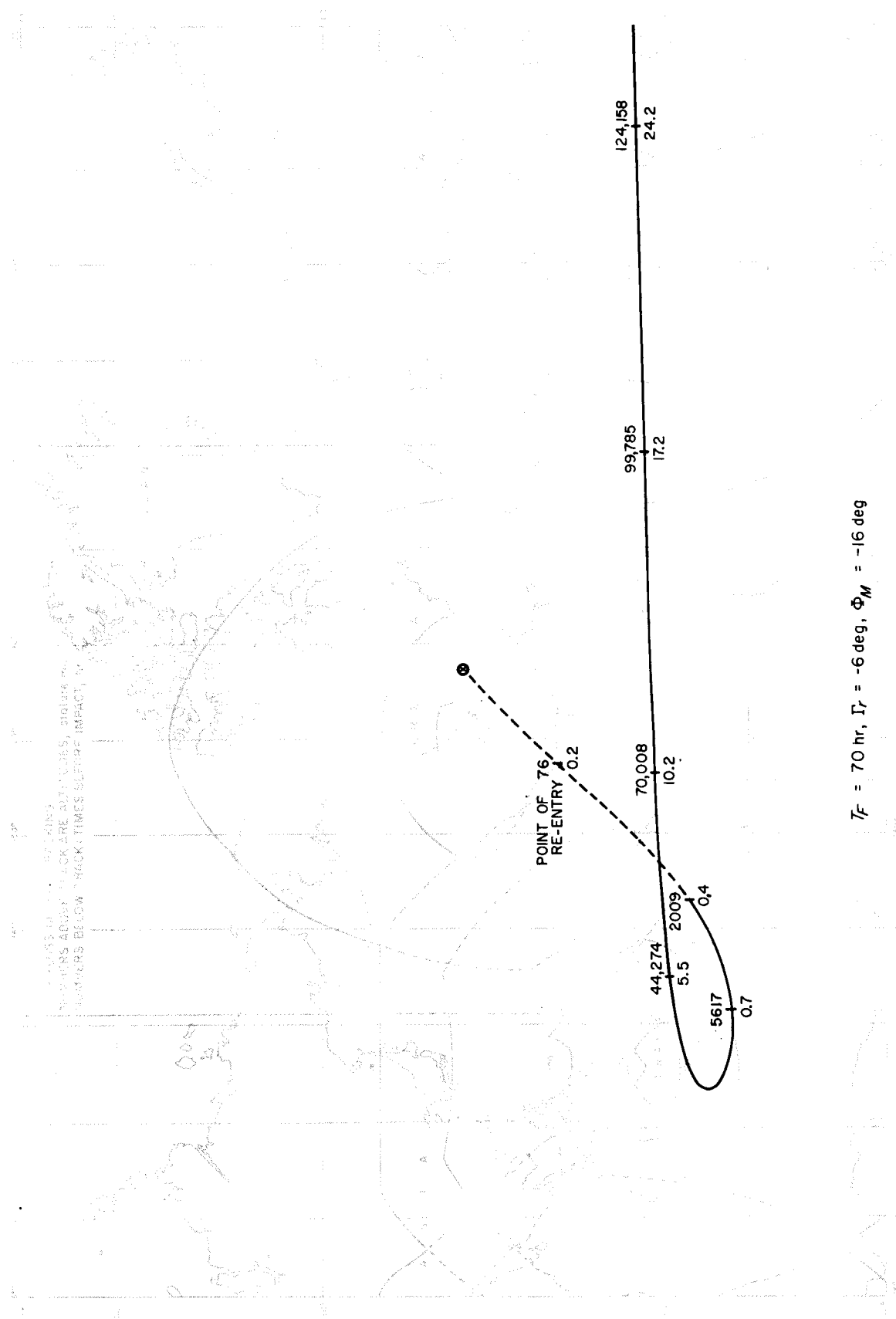
C. Launch-on-Time Theory

The launch-on-time problem consists of launching a space vehicle at the proper time, given a certain launch azimuth, so that a particular set of terminal conditions is met. In the case of Earth-to-Moon missions, there is a very strong relationship between launch time and launch azimuth because of the rotation of the Earth. The trajectory plane must contain the outward radial direction, S , which is fixed in space at a particular inclination to the equatorial plane. As a result, launch must occur when the launch site passes through the space-fixed plane. Since the launch site is rotating with the Earth at a speed of about 0.25 deg/min, a delay in launch time causes the

trajectory plane to rotate about the Earth's spin axis away from the desired outward radial direction.

In the case of Moon-to-Earth missions, the Moon is rotating at a considerably slower rate than the Earth, which simplifies the launch-on-time problem. Delays in the launch time in the order of minutes change the trajectory plane very little so that the actual outward radial direction is nearly the same as the desired outward radial direction. However, significant error occurs in the impact site longitude. If a delay of Δt occurs in the launch time, then the actual impact site is not the desired impact site, as a result of the rotation of the desired impact site from the nominal location in inertial space. The angular rotation is equal to the rotation of Earth relative to the Moon in time Δt , $\Delta t_f (\omega_E - \omega_{EM})$, and is equal to about 8.0 deg for a firing window of 30 min. In order to achieve the desired impact site, a correction ΔT_F is made for this error and corrections $\Delta(B \cdot T)$ and $\Delta(B \cdot R)$ are made for errors in the outward radial direction by means of a midcourse maneuver.

As a result of the importance of accuracy in the impact site, assuring the safety of the astronauts, a second correction is made during re-entry into the Earth's atmosphere. This is accomplished by controlling the re-entry trajectory by means of a retromaneuver at re-entry or by aerodynamic flying during re-entry or by both. Figure 32 presents the nominal trajectory and the corrected trajectory as a line of arrows and a dashed line, respectively. The corrected trajectory is required because of the errors in $\Delta\theta$ and $\Delta\phi$ not corrected for by the midcourse maneuver. The corrections required are out-of-plane maneuver angles of Σ_r' and η_r' . The re-entry maneuver is purely a precision maneuver and is not intended to correct for large errors in $\Delta\phi$ and $\Delta\theta$, as is the midcourse maneuver.



$T_F = 70 \text{ hr}$, $\Gamma_r = -6 \text{ deg}$, $\Phi_M = -16 \text{ deg}$

Fig. 13. Lunar return Earth track for launch date of March 8, 1969, and landing site at San Antonio, Texas

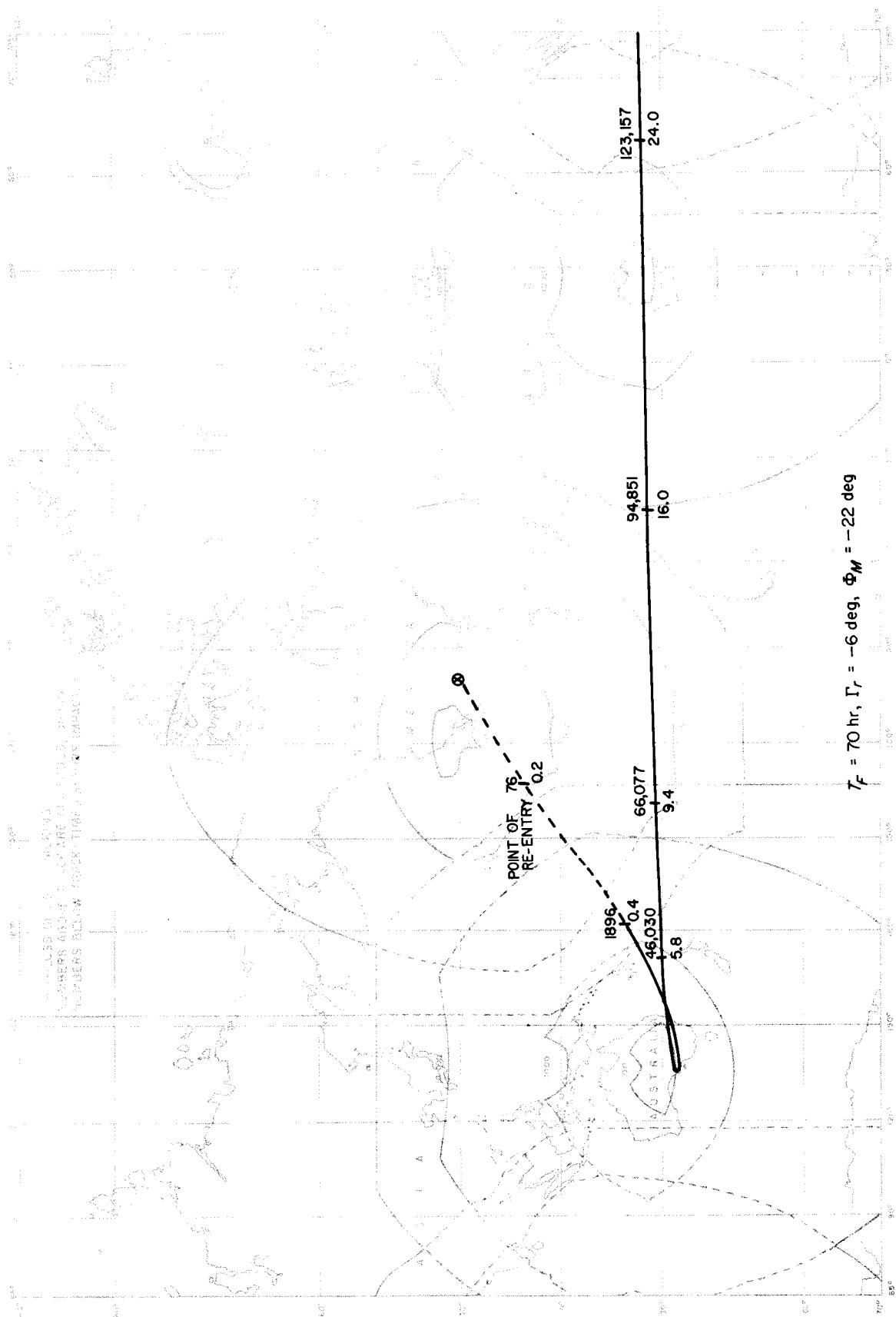


Fig. 14. Lunar return Earth track for launch date of March 9, 1969, and landing site at San Antonio, Texas

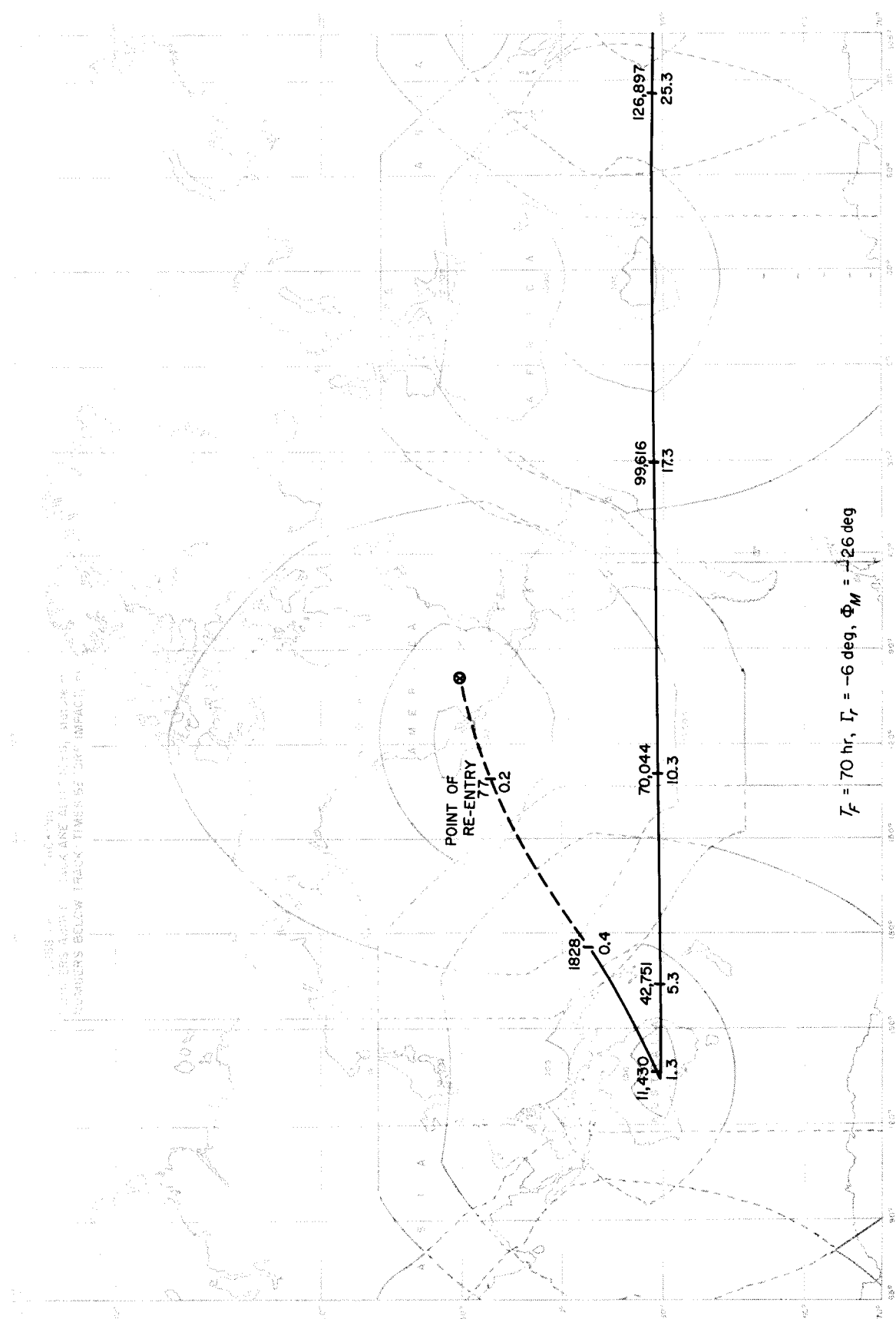


Fig. 15. Lunar return Earth track for launch date of March 10, 1969, and landing site at San Antonio, Texas

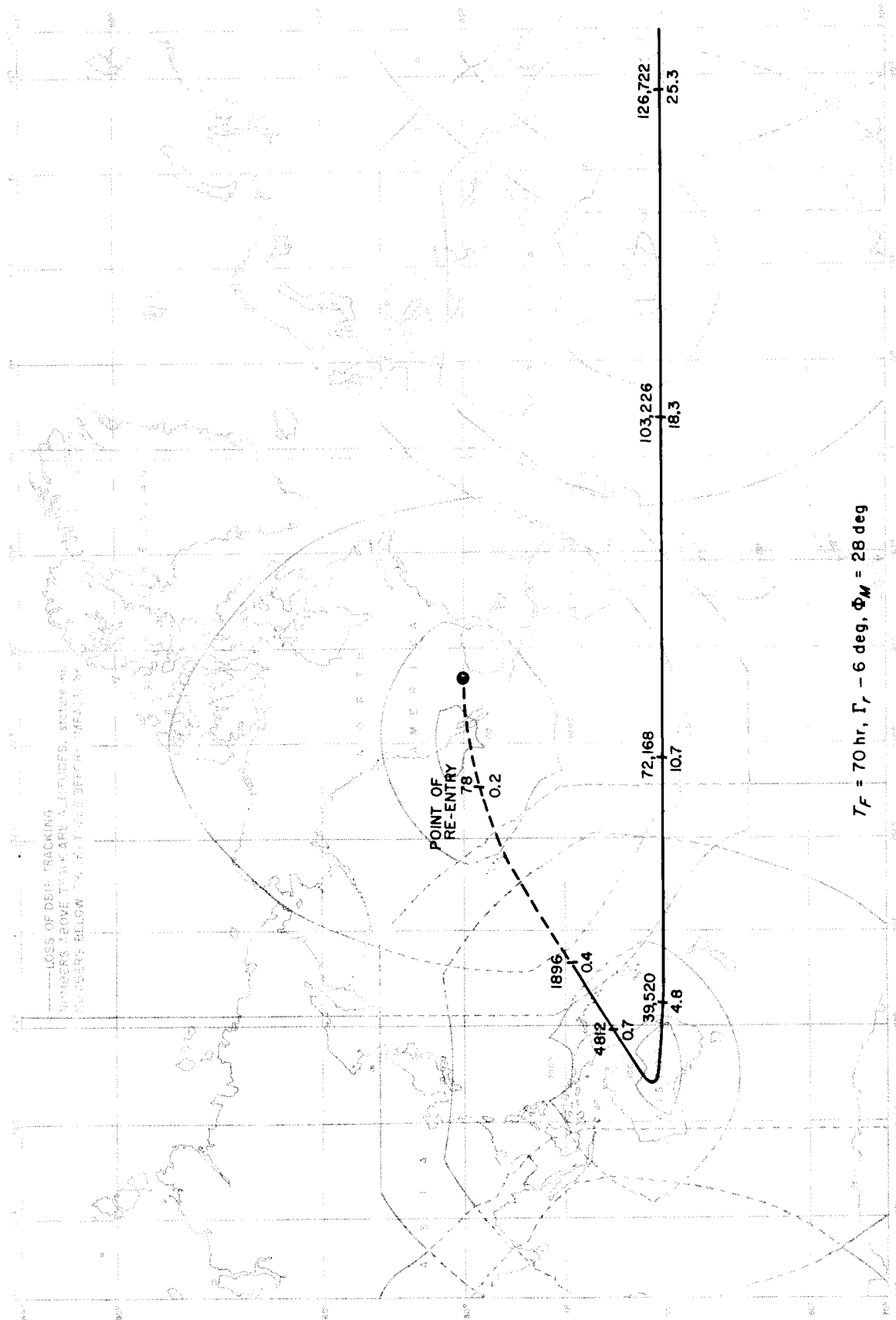


Fig. 16. Lunar return Earth track for launch date of March 11, 1969, and landing site at San Antonio, Texas

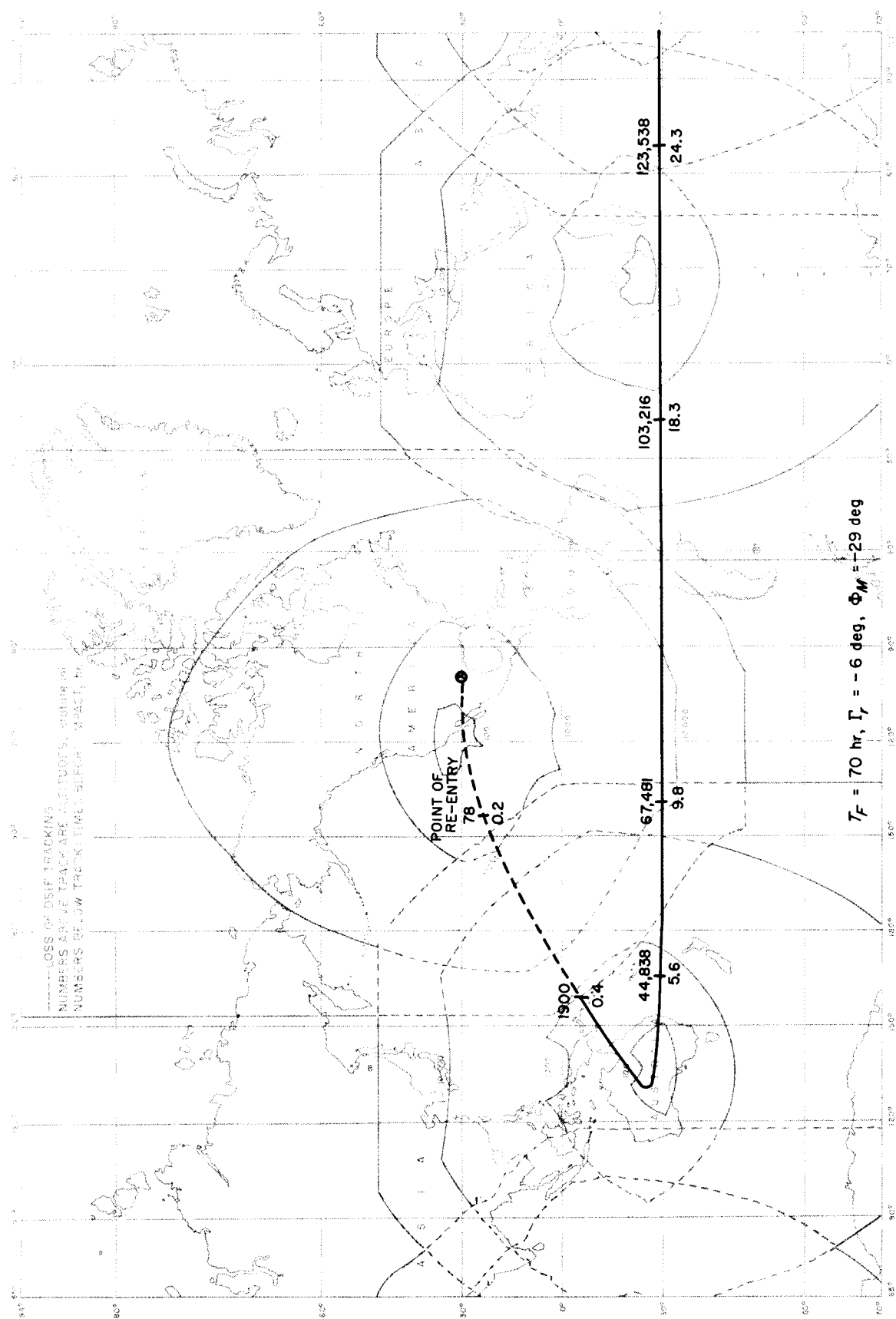


Fig. 17. Lunar return Earth track for launch date of March 12, 1969, and landing site at San Antonio, Texas

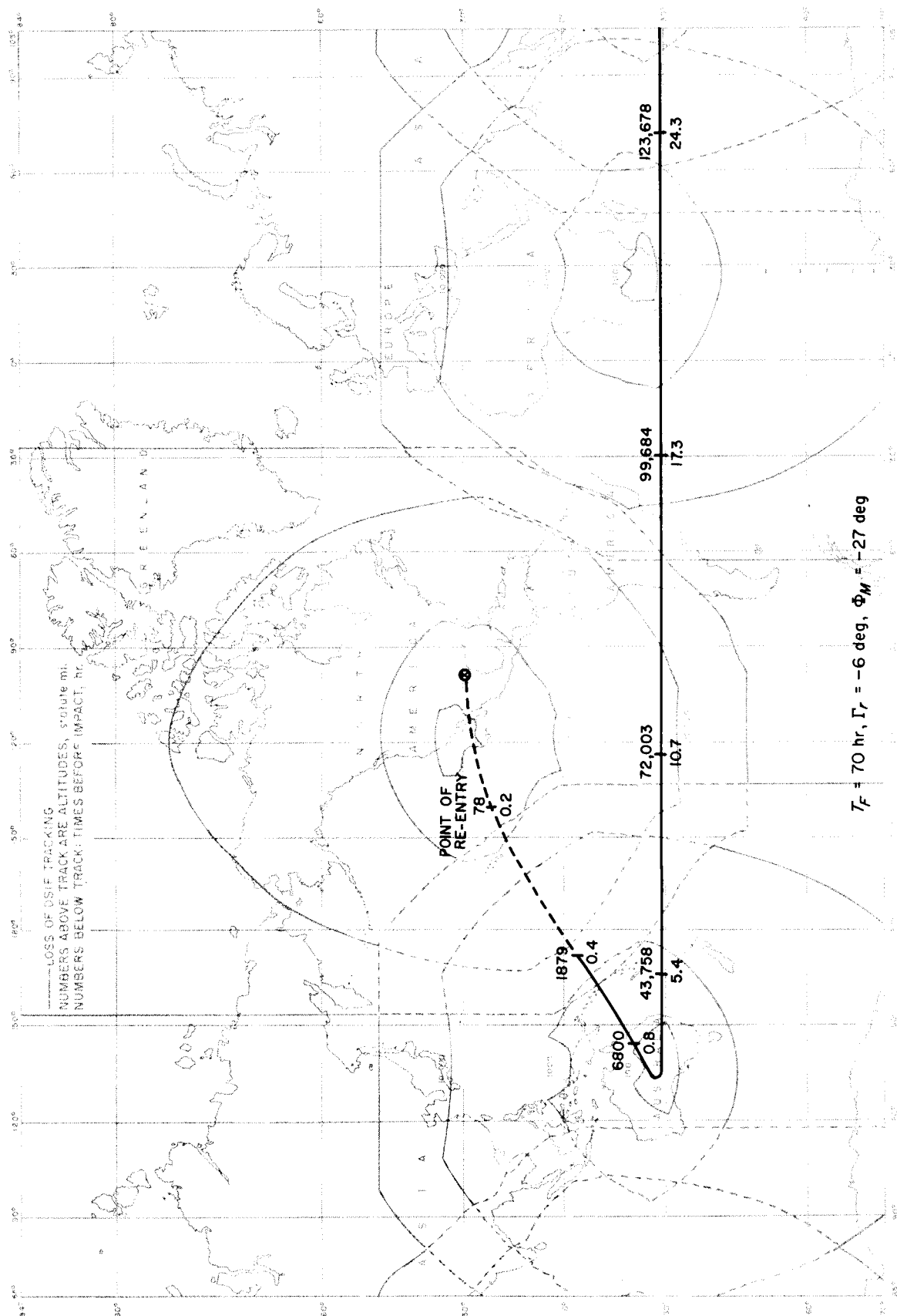


Fig. 18. Lunar return Earth track for launch date of March 13, 1969, and landing site at San Antonio, Texas

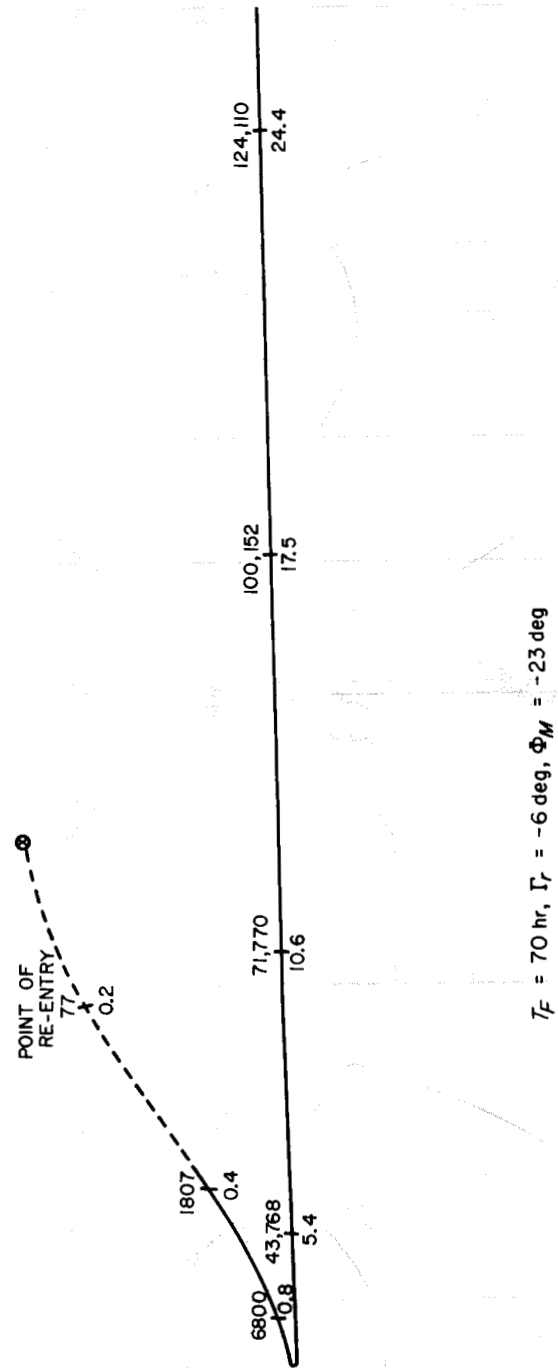


Fig. 19. Lunar return Earth track for launch date of March 14, 1969, and landing site at San Antonio, Texas

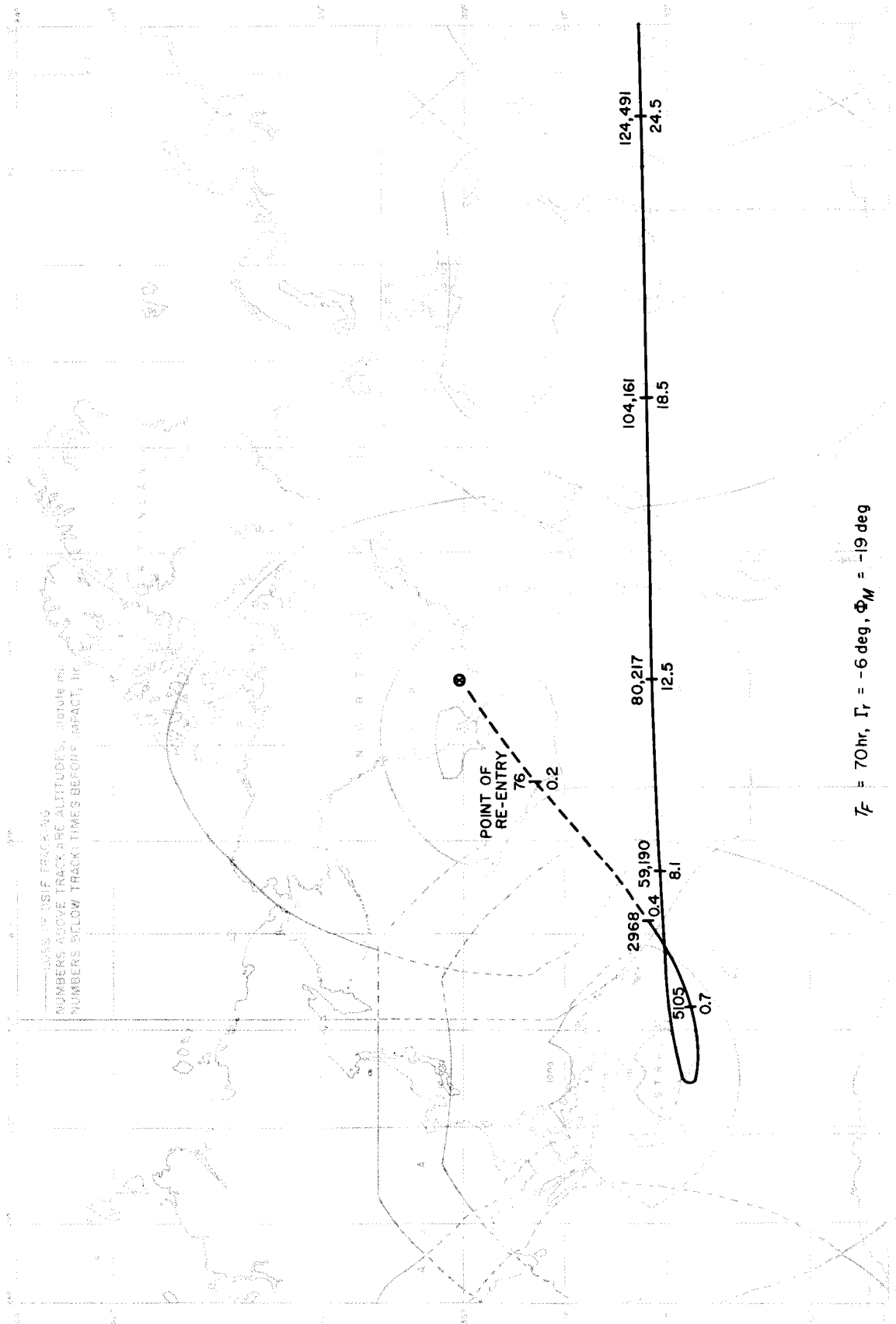


Fig. 20. Lunar return Earth track for launch date of March 15, 1969, and landing site at San Antonio, Texas

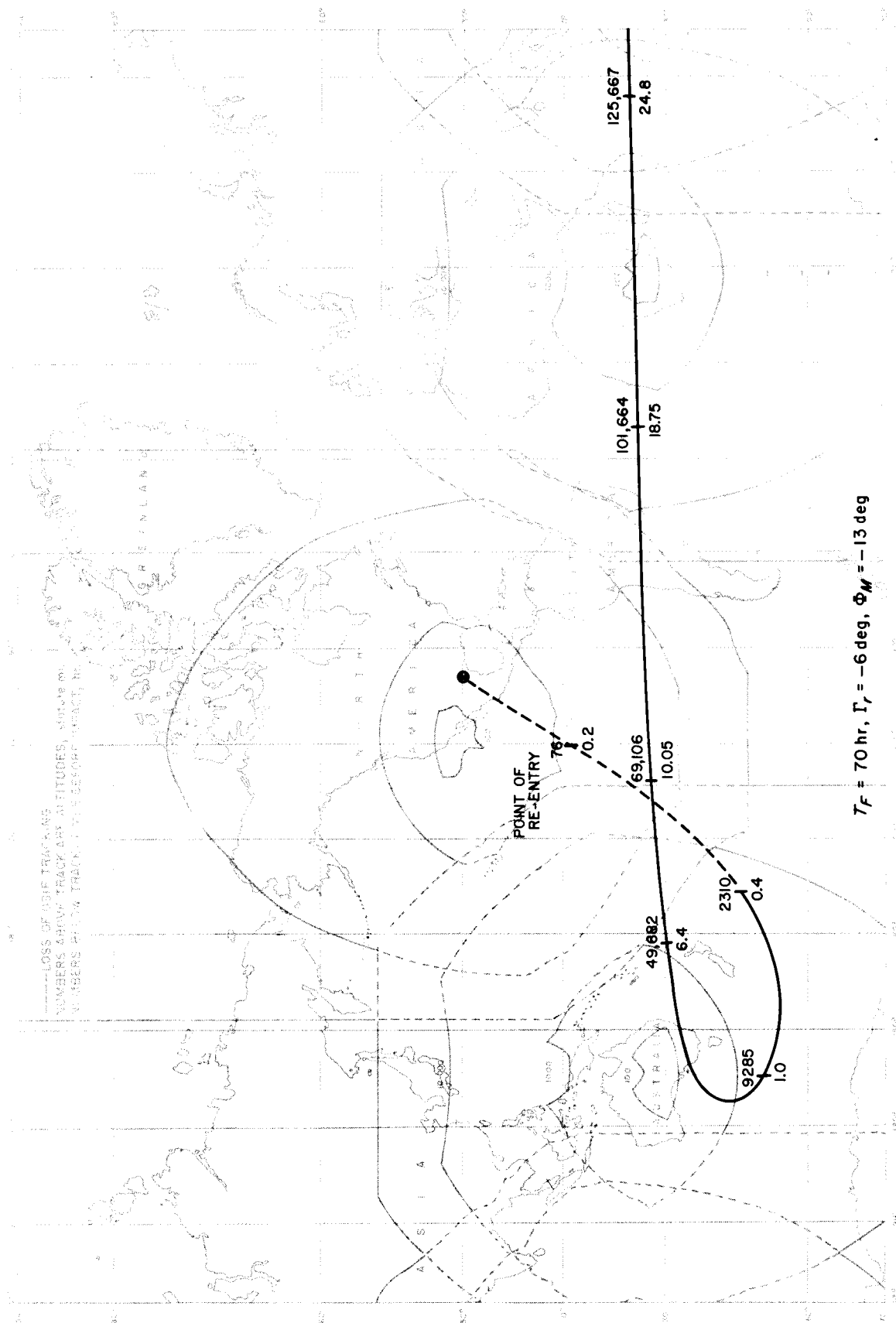


Fig. 21. Lunar return Earth track for launch date of March 16, 1969, and landing site at San Antonio, Texas

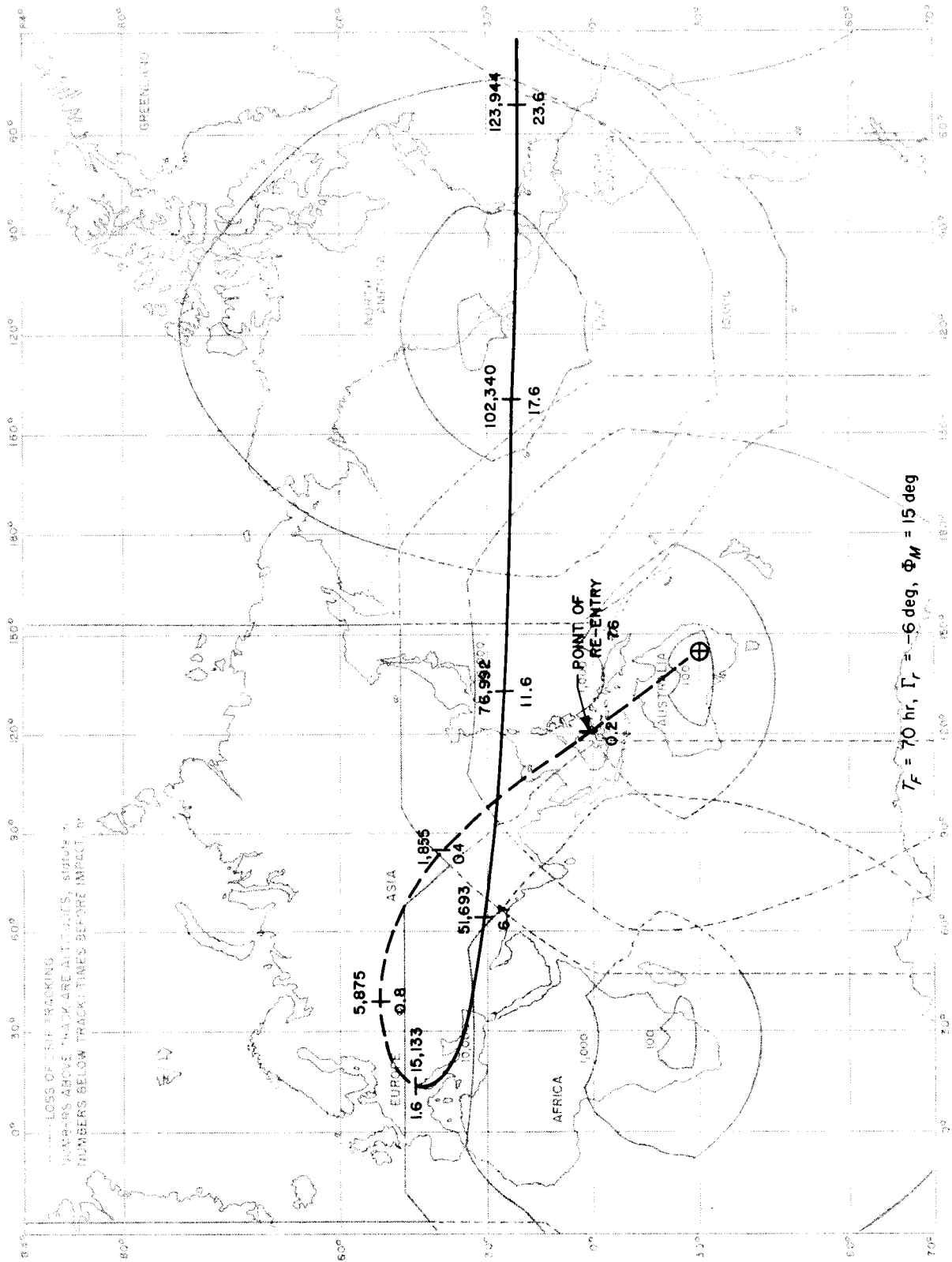
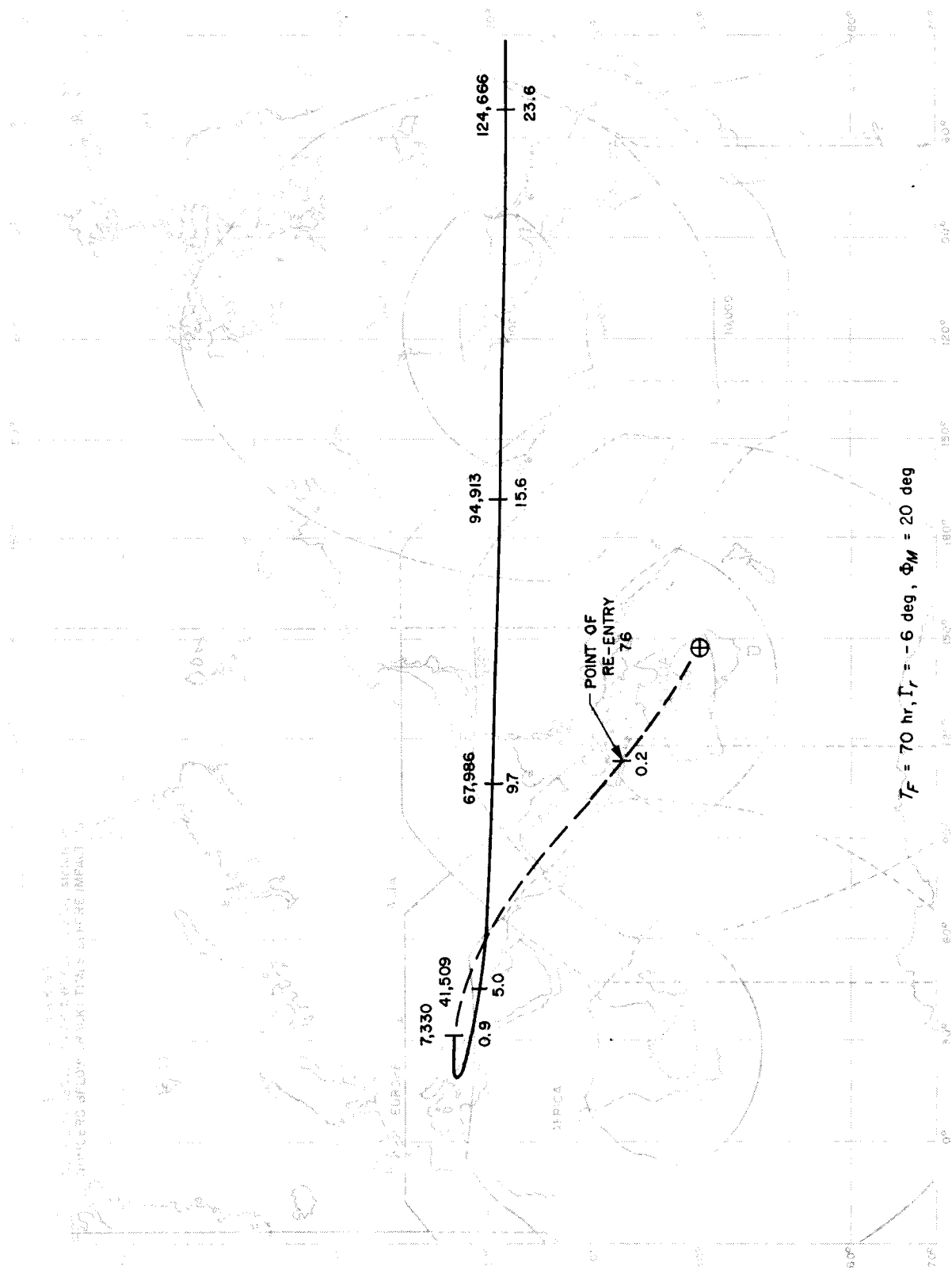


Fig. 22. Lunar return Earth track for launch date of March 20, 1969, and landing site at Bourke, Australia



$T_F = 70 \text{ hr}$, $\Gamma_r = -6 \text{ deg}$, $\Phi_M = 20 \text{ deg}$

Fig. 23. Lunar return Earth track for launch date of March 21, 1969, and landing site at Bourke, Australia

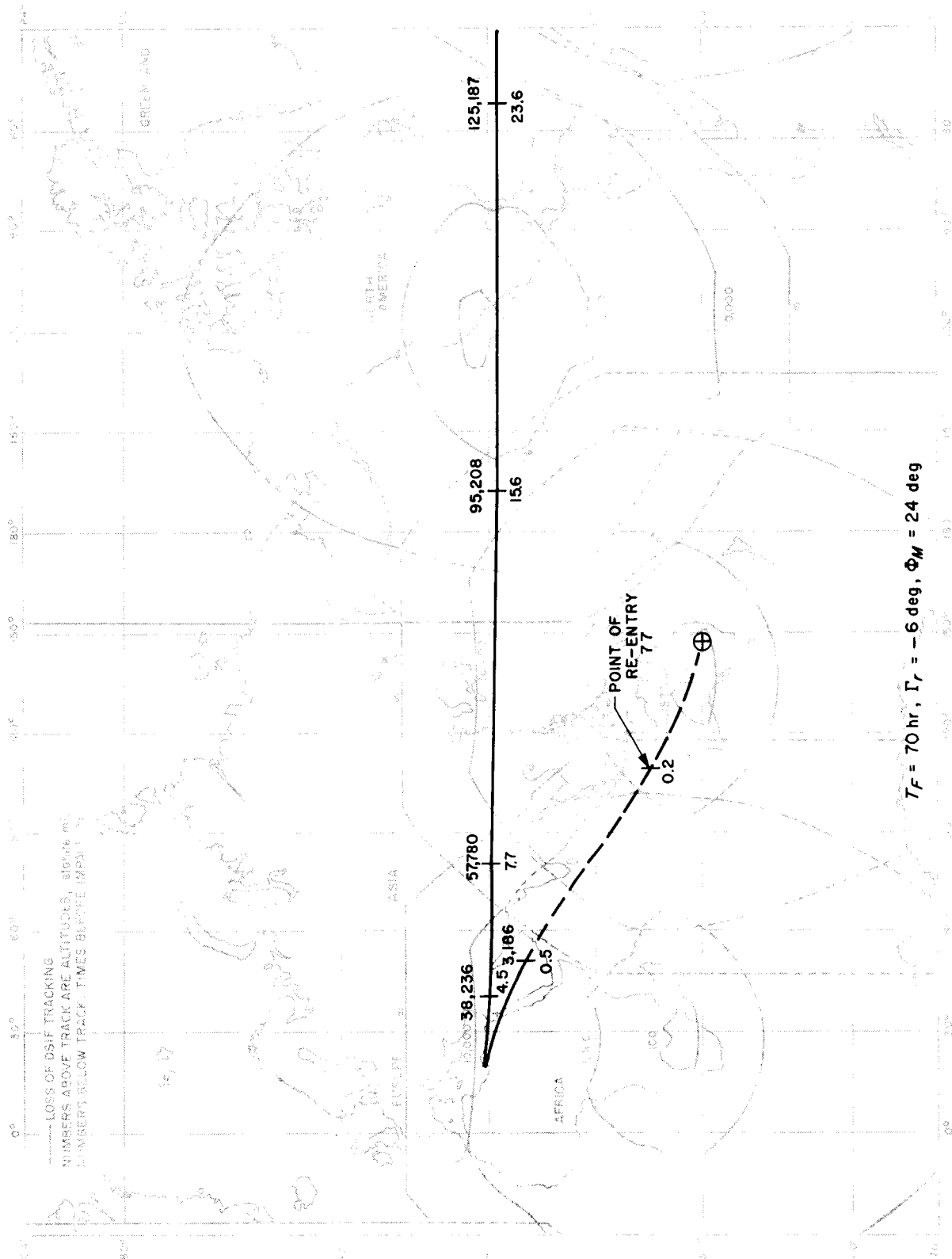


Fig. 24. Lunar return Earth track for launch date of March 22, 1969, and landing site at Bourke, Australia

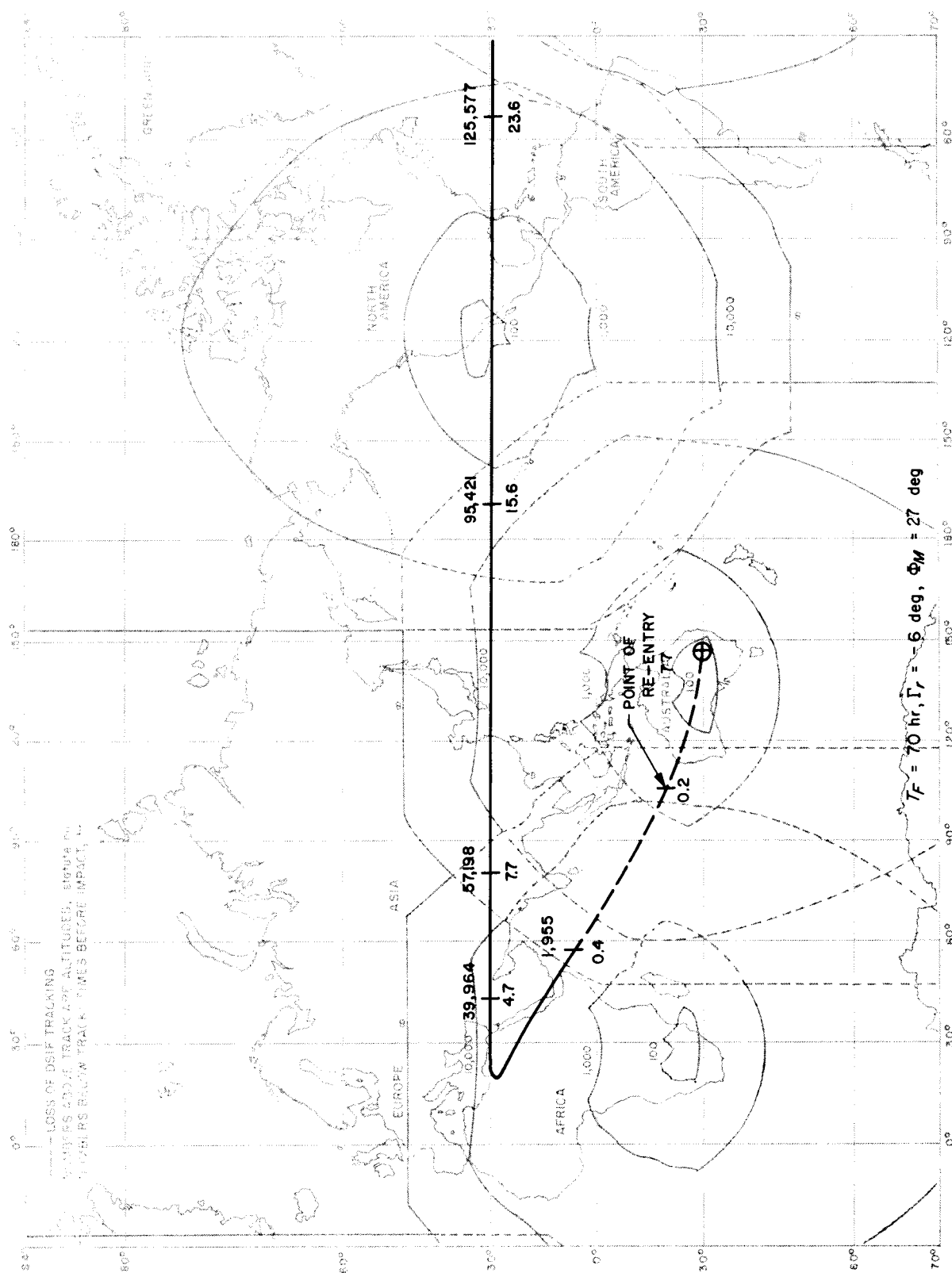


Fig. 25. Lunar return Earth track for launch date of March 23, 1969, and landing site at Bourke, Australia

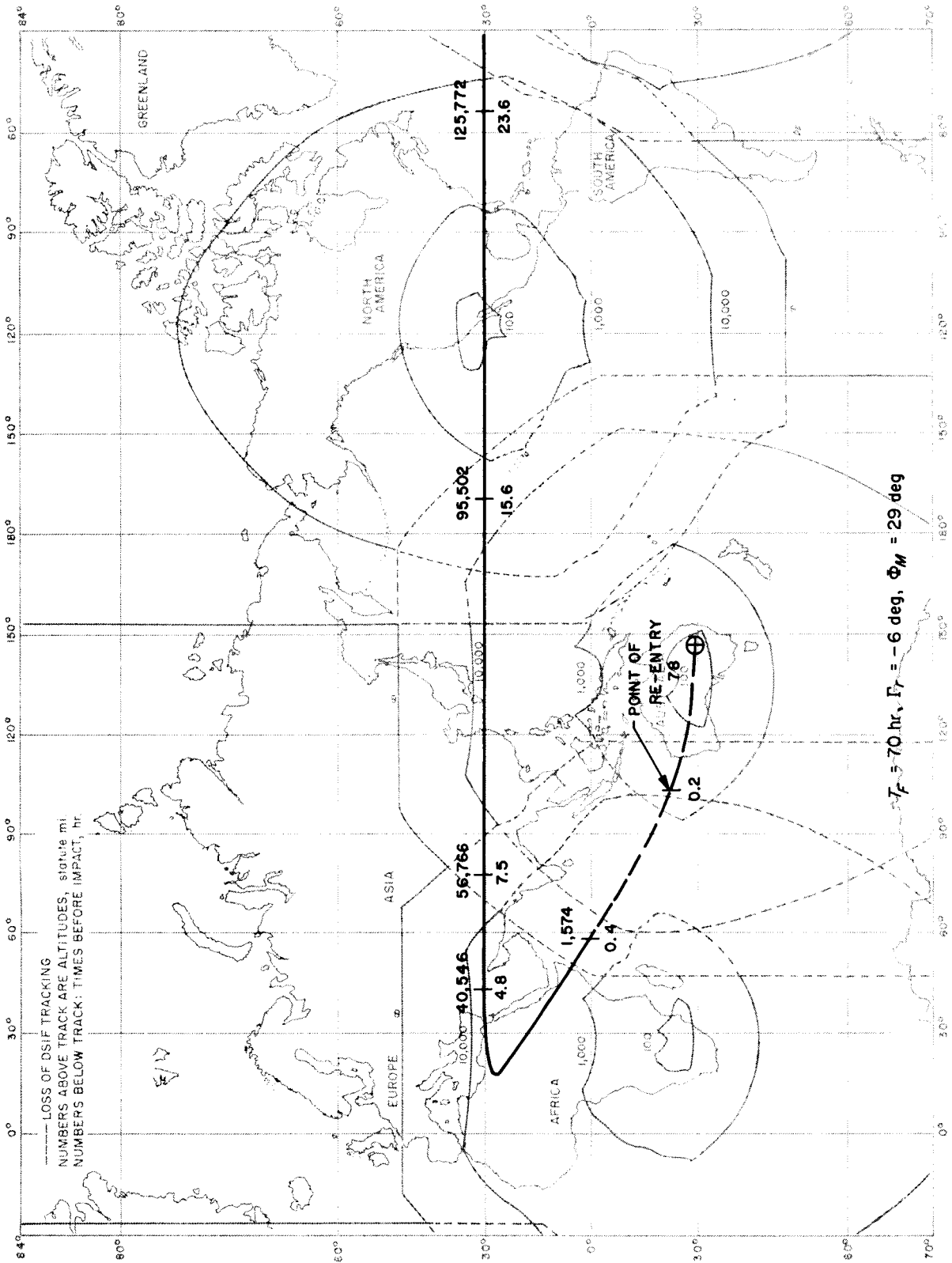


Fig. 26. Lunar return Earth track for launch date of March 24, 1969, and landing site at Bourke, Australia

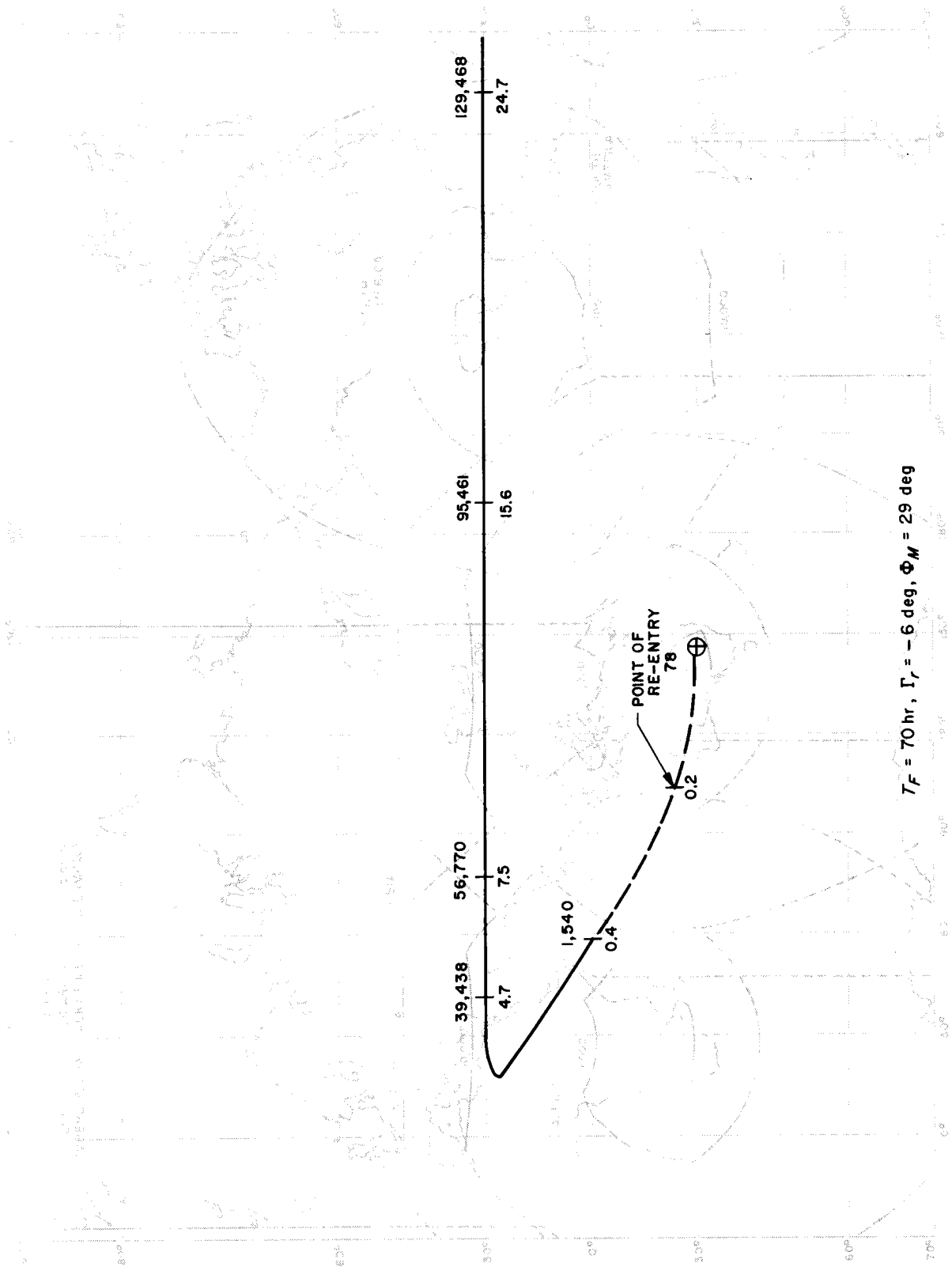


Fig. 27. Lunar return Earth track for launch date of March 25, 1969, and landing site at Bourke, Australia

Fig. 28. Lunar return Earth track for launch date of March 27, 1969, and landing site at Bourke, Australia

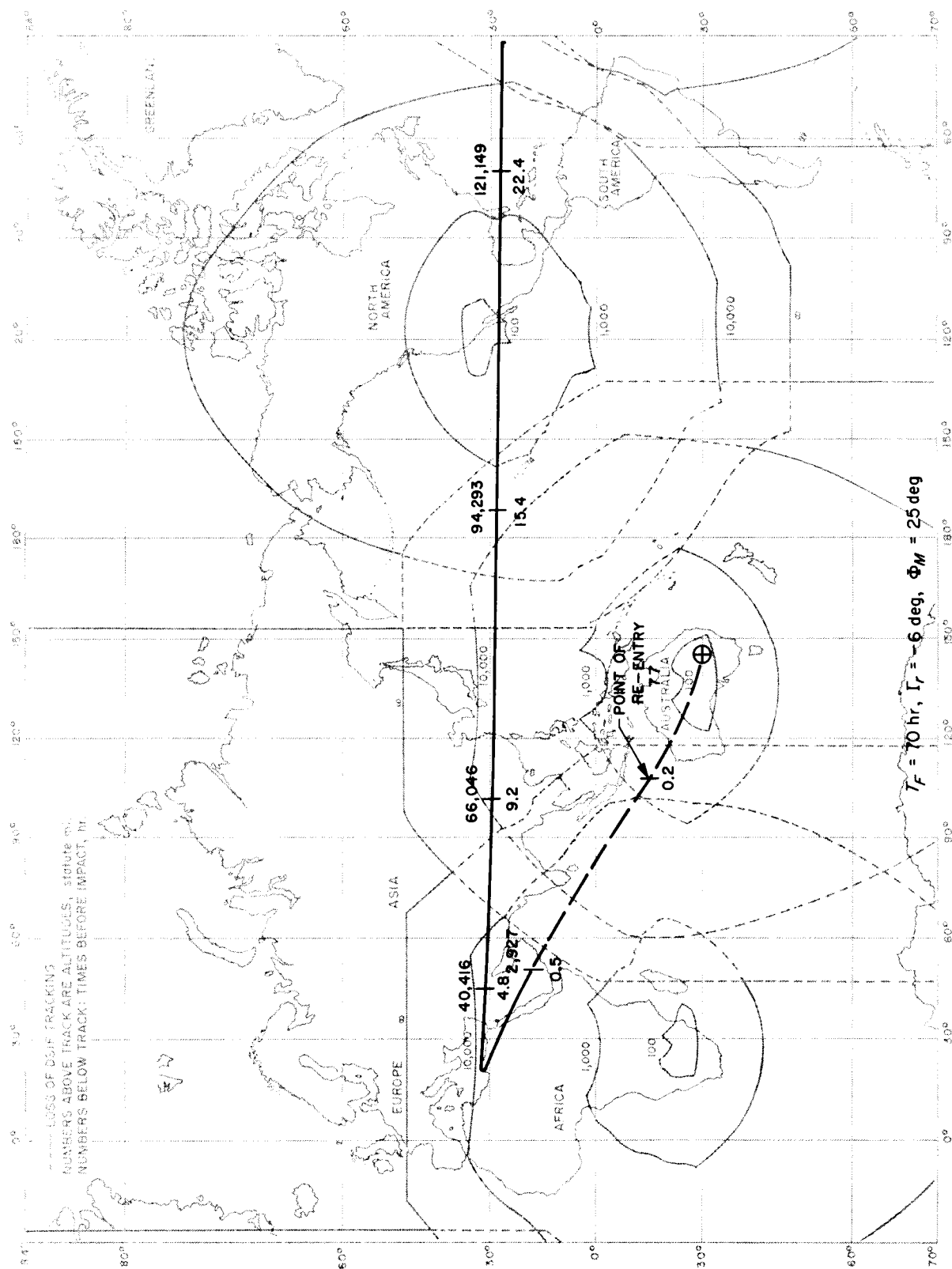


Fig. 29. Lunar return Earth track for launch date of March 28, 1969, and landing site at Bourke, Australia

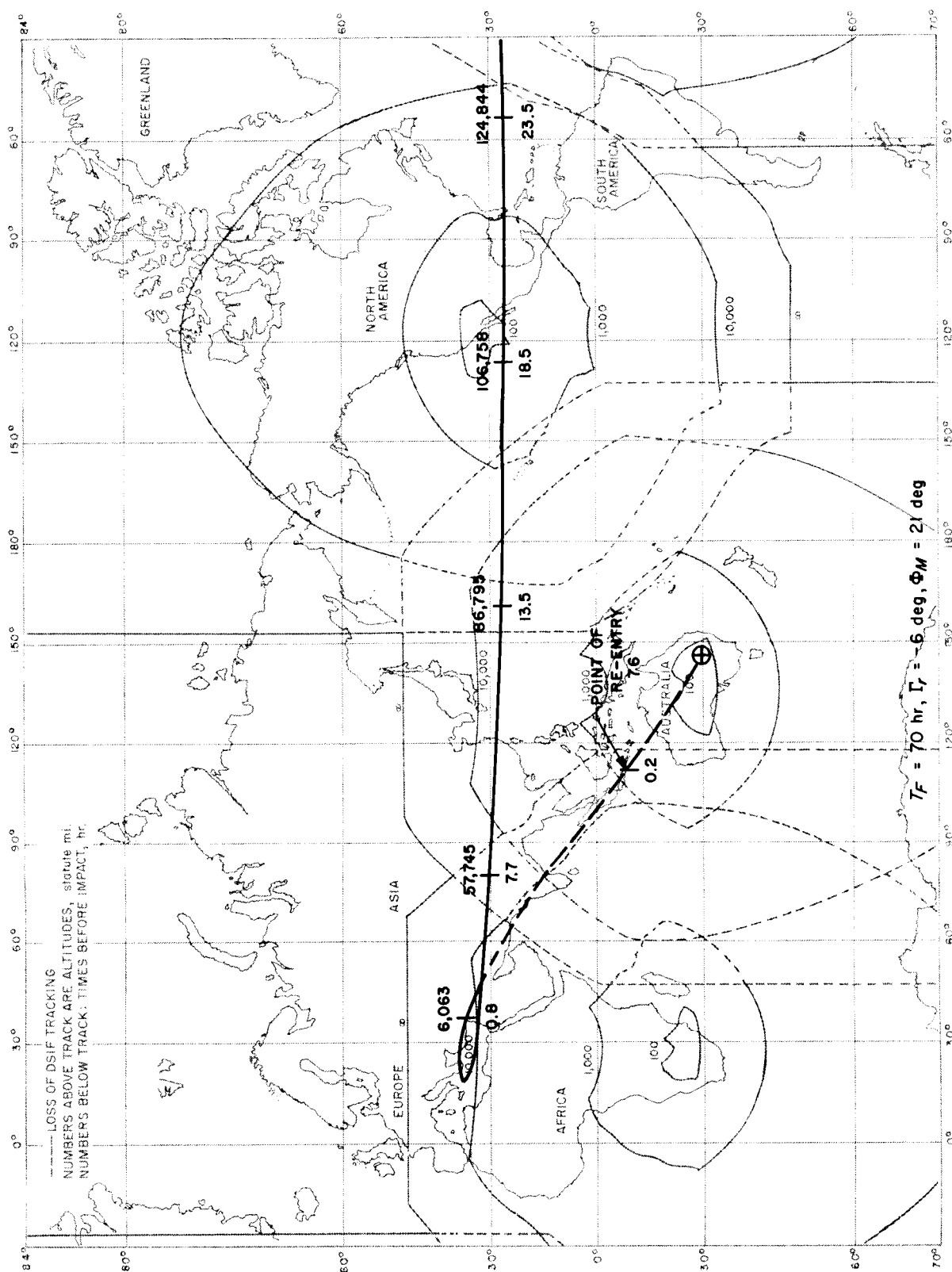


Fig. 30. Lunar return Earth track for launch date of March 29, 1969, and landing site at Bourke, Australia

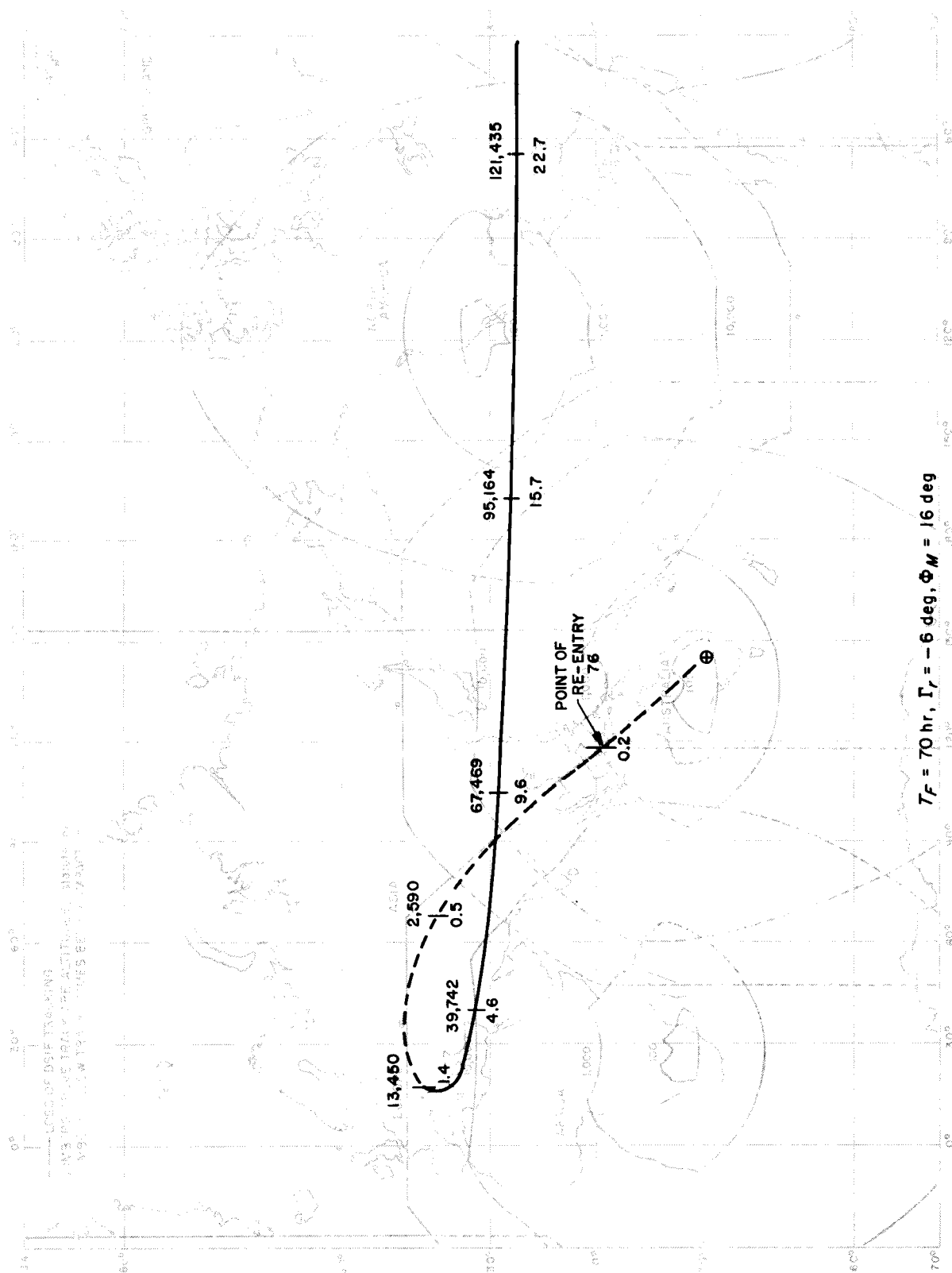


Fig. 31. Lunar return Earth track for launch date of March 30, 1969, and landing site at Bourke, Australia



Fig. 32. Launch-on-time problem

NOMENCLATURE

Definitions

Ascent trajectory. The initial phase of a trajectory, usually consisting of the powered flight. The ascent trajectory begins at the launch point and terminates at the burn-out of the last stage of large impulse (excludes mid-course maneuvers, etc.).

Clockwise re-entry. Re-entry into the atmosphere of a body in the opposite direction as its rotation.

Counterclockwise re-entry. Re-entry into the atmosphere of a body in the same direction as its rotation.

Firing window. The time interval in any one day during which firings may be attempted (hr).

Keplerian orbit. The motion of one body in an inverse-square force field of a second larger body. Also called conic motion.

Launch period. The number of consecutive days on which launchings may be attempted.

Launch time, t_l . The time at which a launching will be attempted. Liftoff time and launch time are interchangeable.

Maneuver angle. The central angle between the re-entry point and the impact point.

Miss distance vectors \mathbf{B} , $\mathbf{B} \cdot \mathbf{T}$, $\mathbf{B} \cdot \mathbf{R}$. Defined in Section III-C.

Outward radial direction. The direction of the outgoing asymptote of the selenocentric hyperbola.

Piercing point or exit point. The point at which a spacecraft passes through the lunar sphere of influence. The point at which the outward radial direction pierces the sphere of influence is very nearly the same point.

Re-entry trajectory. The terminal phase of a trajectory. That phase of flight which occurs within the atmosphere of the target body. The re-entry trajectory begins at the re-entry point and terminates at the impact point.

Sphere of influence. The locus of points about body 1 at which the ratio between the force with which body 2 perturbs the motion of body 3 and the force of attraction of body 1 is equal to the ratio between the force with which body 1 perturbs the motion of body 3 and the force of attraction of body 2. The radius of this sphere for the Moon is equal to $0.87 (r_{ME}) (M_M/M_E)^{2/5}$.

Transfer orbit. The intermediate phase of a trajectory. The transfer orbit begins at the injection point and terminates at the re-entry point.

Subscripts

- b burnout point
- ca closest approach
- E quantities referring to the Earth
- i impact point
- ℓ launch point
- M quantities referring to the Moon
- p point of closest approach
- r re-entry point
- ' (prime mark) corrected trajectory
- s point of exit from sphere of influence

Symbols

Vectors are indicated by boldface type.

- a semimajor or semitransverse axis
- \mathbf{B} impact parameter
- $\mathbf{B} \cdot \mathbf{R}$ projection of the impact parameter \mathbf{B} upon the vector \mathbf{R}
- $\mathbf{B} \cdot \mathbf{T}$ projection of the impact parameter \mathbf{B} upon the vector \mathbf{T}
- C_3 twice the total energy per unit mass;
 $C_3 = V^2 - 2GM/r$
- e eccentricity
- G gravitational constant
- i inclination
- M mass of a body
- p point of closest approach
- \mathbf{P} a unit vector from the central body to the point of closest approach
- \mathbf{Q} a unit vector perpendicular to \mathbf{P} and lying in the trajectory plane
- \mathbf{r} a vector directed from the center of the central body to a second body. For example, \mathbf{r}_{EM} is the vector from the Earth to the Moon and r_{EM} is its magnitude.
- \mathbf{R}_l a vector directed from the center of the central body to the launch site
- \mathbf{R} a unit vector which forms the right-handed system $\mathbf{R}, \mathbf{S}, \mathbf{T}$. $\mathbf{R} = \mathbf{S} \times \mathbf{T}$

S a unit vector in the direction of the incoming asymptote for an escape hyperbola or the outgoing asymptote for an escape hyperbola (outward radial direction). In the case of an ellipse, a pseudoasymptote is defined, see Section III-C.

T a unit vector perpendicular to **S** that lies in the equatorial plane

T_F the time of flight from launch to impact

t time of injection

t_l launch time

V inertial speed with respect to the central body

V_P inertial velocity of the probe relative to the Earth

V_{PM} inertial velocity of the probe relative to the Moon

V_M inertial velocity of the Moon relative to the Earth

W a unit vector which forms the right-handed system **P**, **Q**, **W**. $\mathbf{W} = \mathbf{P} \times \mathbf{Q}$

Γ inertial flight-path angle with respect to the local horizontal, measured in a positive direction away from the central body

η an angle measured in the plane of the trajectory

η_{r0} true anomaly of re-entry

θ longitude measured eastward

θ_s the angle between the closest approach direction **P** and the outward radial direction **S**

Σ inertial azimuth measured east from true north

Φ_M declination of the Moon at launch

φ latitude

ω_E rotation rate of the Earth about its axis

ω_{EM} rotation rate of the Moon about the Earth

Units of Measurement

The units used throughout this Report, except for the Earth tracks and associated data, are as follows:

Distance kilometers

Speed kilometers/second

Energy kilometers²/second²

Angular momentum kilometers²/second

Time Greenwich mean time or hours

Angles degrees

Equivalence signs

\cong approximately equal to

\triangleq equal by definition

REFERENCES

1. Penzo, P. A., *An Analysis of Moon-to-Earth Trajectories*, Report 8976-0008-RU-000, Space Technology Laboratories, Inc., Redondo Beach, California, October 30, 1961.
2. Clarke, V. C., Jr., *Design of Lunar and Interplanetary Ascent Trajectories*, Technical Report No. 32-30, Jet Propulsion Laboratory, Pasadena, California, March 15, 1962.
3. Penzo, P. A., Kliger, I., and Tonies, C. C., *Analytic Lunar Return Program, Computer Program Guide*, Report 8976-0005-MU-000, Space Technology Laboratories, Inc., Redondo Beach, California, August 23, 1961.
4. Holdridge, D. B., *Space Trajectories Program for the IBM 7090 Computer*, Technical Report No. 32-223, Jet Propulsion Laboratory, Pasadena, California, March 2, 1962.
5. Dallas, S. S., *Two Search Routines for Computing Lunar Return Trajectories*, Section 312 Request for Programming No. 72, Jet Propulsion Laboratory, Pasadena, California, June 26, 1962.
6. Kizner, W., *A Method of Describing Miss Distance for Lunar and Interplanetary Trajectories*, External Publication No. 674, Jet Propulsion Laboratory, Pasadena, California, August 1, 1959.

ACKNOWLEDGMENTS

The author wishes to acknowledge the suggestions of V. C. Clarke and D. Richardson. Mr. Clarke provided assistance in the theory of lunar return trajectories and Mr. Richardson provided assistance on the search routines and did all the actual programming. Work done by P. A. Penzo under contract to JPL is described in Ref. 1, 3. This work served as the starting point for some of the results described in this Report.